Influence of Nanoscale Surface Modifications on the Fatigue Resistance of Medically Relevant Metals

Amirhossein Ketabchi, B.A.Sc.

Thesis Submitted to the

Faculty of Graduate and Postdoctoral Studies

in partial fulfillment of the requirements

for the M.A.Sc degree in Mechanical Engineering

Ottawa-Carleton Institute for

Mechanical and Aerospace Engineering

University of Ottawa

Master of Applied Science (2013), University of Ottawa

(The Ottawa-Carleton Institute for
Mechanical and Aerospace Engineering) Ottawa, Ontario

Title: Influence of nanoscale surface modifications on the fatigue resistance of medically relevant metals

Author: Amirhossein Ketabchi
Supervisor: Dr. Arnaud G. Weck
Co-supervisor: Dr. Fabio Variola

Number of pages: xiii, 108

In the name of God the compassionate the merciful

Acknowledgments

First and foremost I would like to express my sincere gratitude to my supervisors Dr. Weck and Dr. Variola, who have supported me throughout the course of completing my Master's degree with their guidance, patience, knowledge, and motivation. I would never have been able to finish my thesis without their support.

I would like to thank Dr. Cao who helped me to carry out fatigue evaluation experiments. I would like to thank my colleague Dr. Asadi for sharing with me his materials science knowledge, and Y. Liu for helping me in microscopic imaging.

Finally, I wish to thank my beloved wife, Saba, who always stood by me through the good times and bad, and my parents for their support.

Abstract

With an increasingly aging population, a significant challenge in implantology is the creation of biomaterials that actively promote and accelerate tissue integration while offering excellent mechanical properties. Engineered surfaces with superimposed micro and nanoscale topographies showed great potential to control and direct biomaterial-host tissue interactions. However, these modified surfaces require a careful assessment to prevent potential adverse effects on the fatigue resistance, a factor which may ultimately cause premature failure of biomedical implants.

In this context, the surfaces of two widely used biocompatible metals, namely CP Ti and Ti-6Al-4V, were engineered through simple yet efficient chemical treatments which demonstrated the ability to confer exciting new bioactive capacities. The qualitative and quantitative assessments of the fatigue resistance of polished and treated metals were carried out. Results from this study highlight the importance of mechanical considerations in the development and evaluation of nanoscale surface treatments for metallic biomedical implants.

Table of Contents

List of figures

List of tables

Chapter 1 Introduction

1.1 Context

Metal implants used for various clinical conditions are relatively effective but they still need significant improvement with respect to their capacity to secure rapid and long-lasting integration in tissues [1]. To address these challenges, different strategies have been developed to design metal surfaces in ways to directly affect the molecular and cellular events at the material-host tissue interface that ultimately determine the biological outcome of biomedical implants [2]. It is in fact well established that implant-host tissue interactions are governed by the micro and nanoscale surface properties of materials, such as topography, roughness, surface chemistry and potential [2][3]. It is therefore evident that achieving the capacity to precisely design the physicochemical makeup of surfaces will ultimately result in the ability to control and guide the biological response to an implanted biomaterial. In this context, various approaches have been developed to rationally modify the surfaces of titanium-based metals, the gold standard in medicine [2] (see section 2.6). In particular, chemical treatments such as oxidative nanopatterning and anodization have shown to be very effective tools to endow titanium-based metals with the ability to guide cellular events [2][3]. This unique capacity results from the creation of distinctive nanoporous surfaces (sponge-like structures in the case of oxidative nanopatterning, and nanotube arrays in the case of anodization) capable of advantageous

physicochemical signaling to adhering cells [4][5]. In addition, these chemical approaches permit to modulate specific surface properties (e.g. topography, roughness and chemical composition), a prerequisite to exert a selective control on cell activities [2][3]. While these treatments showed promising biological results, it is now critical to determine whether the mechanical properties are affected. One can in fact argue that the topographical modifications introduced by these two methods may act as stress raisers and negatively impact the fatigue resistance of treated metals. If this were to be true, the applicability of these approaches to biomedical implants, which are normally subject to intense and complex stress fields, will have to be reconsidered. In particular, while modifying surface topography and roughness are promising to promote bone ingrowths and therefore improve bone integration, it may affect the mechanical properties such as fatigue resistance. Increasing surface roughness will result in generating pores and cracks that can be regarded as small notches on the surface of the material. These features may be expected to create stress concentration on a material's surface. Possible stress concentrations on the surface are crack initiation sites that lead to higher failure rates in materials. Material failure can be classified in various types from which fatigue failure is counted as one of the most crucial ones. Fatigue failure is reported to account for about 90% of all failures in metals, polymers, and ceramics [6]. Similarly, biomaterial fatigue failure is a common type of failure in biomedical devices [6]. For instance, in dental implants, removable partial denture framework, clasps, plates, pedicle screws and cables fatigue are one of the main causes of failure [7]. This kind of failure can also be found in orthopedic implants during body motion where implant is subjected to cyclic loads.

1.2 Aim of the Thesis

The main objective of this thesis is thus to study the effects of various surface treatments on fatigue resistance of biocompatible metals. In particular, my research aims at assessing the effects of anodization and oxidative nanopatterning (see sections 2.6.2 and 2.6.3) on the fatigue resistance of commercially pure grade 2 titanium, hereafter indicated as CP Ti, and the titanium alloy Ti-6Al-4V. To achieve these objectives, polished CP Ti and Ti-6Al-4V samples were subjected to the two different chemical treatments. The Piranha solution was used for oxidative nanopatterning, which yielded the creation of a homogeneously distributed network of nanopits. In addition, polished samples of both materials were anodized in a solution of 0.5% hydrofluoric acid, which created uniformly distributed arrays of nanotubes. Polished and chemically treated CP Ti and Ti-6Al-4V samples were divided into six experimental groups (see table 6) and tested to determine their fatigue resistance. Results from this analysis permitted to generate S-N (stress-number of cycles to failure) curves for each experimental group. The S-N curves were analyzed and compared in order to assess the effects of each treatment on fatigue life. Additionally, utilizing the scanning electron microscope (SEM), the effects of fatigue failure on the surface topographies (nanotubes in case of anodization and nanopits in case of oxidative nanopatterning) have been investigated.

Distinctively from previous studies, we have assessed for the first time the influence of oxidative nanopatterning, which is considered as a new method to improve the biocompatibility, on the fatigue resistance of CP Ti and Ti-6Al-4V and compared the results with those of anodized and polished.

The effects of anodization of the fatigue resistance of titanium alloys and pure titanium have been assessed by previous work independently [8][9][10]. However, in this study we have

compared the fatigue behavior of surface modified pure titanium and titanium alloy Ti-6Al-4V. Finally, the effect of cyclic loading on the anodized oxide layer of CP Ti and Ti-6Al-4V was explored.

Chapter 2 Literature review

2.1 Titanium, biomaterial of today

Titanium and its alloys are among the most widely used metals in biomedical applications [7]. Ti-based metals exhibit excellent mechanical and corrosion properties, and outstanding biocompatibility [11]. These advantageous characteristics have made Ti-based metals better choices than other metals such as stainless steel and cobalt-chromium for biomedical applications. Corrosion resistance of titanium and its alloys, which results in better corrosion-fatigue behavior of these materials in physiological environment, is superior to stainless steel and CoCr alloys [7]. Table 1 illustrates mechanical properties of the most common metals used in biomedical applications.

Table 1. Properties of mostly used metals in biomedical applications [12][13].

Material	UTS (MPa)	Yield strength (MPa)	Modulus of elasticity (GPa)	Endurance limit (MPa)	% Elong.
316L SS	490	190	193	210	40
CoNiCrMo	793	241	232	500	50
CP Ti (grade 2)	550	200	105	120	24
Ti-6Al-4V	860	795	116	510	10

2.1.1 Fundamental properties

The excellent corrosion resistance of titanium and its alloys is due to a native protective oxide layer [14], which acts as a barrier between the underlying metal and the corrosive environment. Titanium shows a hexagonal-closed pack (HCP) crystal structure. At 882˚C this transforms into a body-centered cubic (BCC) structure [15]. The crystal structure of titanium will not experience any other transformations up to the melting temperature at 1670˚C [16]. Titanium's Young's modulus is almost half that of stainless steel. Although higher elastic modulus is regarded as a beneficial mechanical property for a metal in most of applications, it should be noted that in orthopedic applications (e.g. femoral stem in a hip prosthesis), the higher the elastic modulus is, the higher the chances of stress shielding will be (i.e. uneven distribution of loads between the bone and the implant, a factor which can cause bone desorption and premature failure of the implant) [7]. The mechanical properties of different grades of titanium and its alloys are reported in table 2. It can be seen that different grades and alloys of titanium exhibit various fatigue behaviors.

Table 2. Titanium alloys properties at room temperature [12].

Material	Grade	Tensile strength (MPa)	Yield strength (MPa)	Modulus of elasticity (GPa)	Endurance limit (MPa)	% Elong.
CP Ti (99.5% Ti)	1	240	170	105	120	24
CP Ti (99.2% Ti)	2	345	275	105	220	20
Ti0.8Ni0.3Mo	12	483	345	108	242	18
Ti3Al2.5V	9	620	483	110	310	15
Ti6Al4V	5	895	828	116	510	10

Figure 1 and figure 2 demonstrate fatigue behavior and endurance limits of CP Ti and Ti-6Al-4V through their S-N curves (stress-number of cycles to failure).

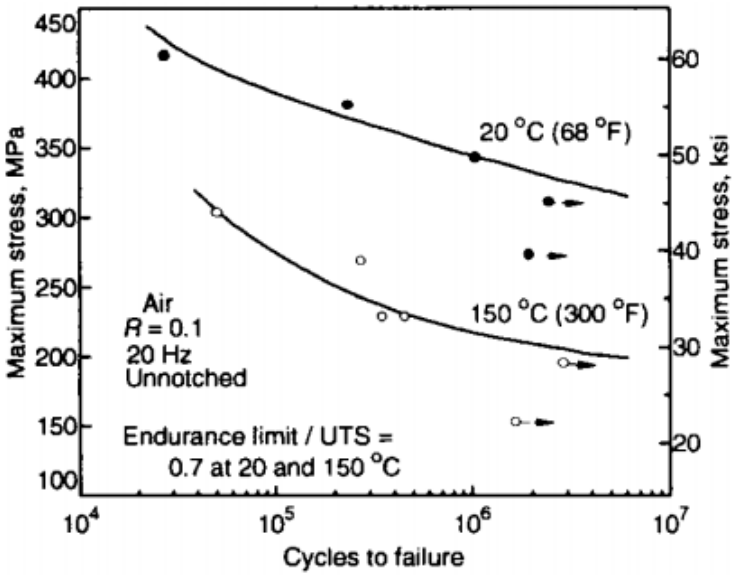

Figure 1. S-N curve of commercially pure grade II titanium fatigue tested in air at temperatures 20˚C and 150˚C. Temperature raise decreased the endurance limit of CP Ti. We are aiming to perform the tests at laboratory temperature which is corresponding to 20˚C [17].

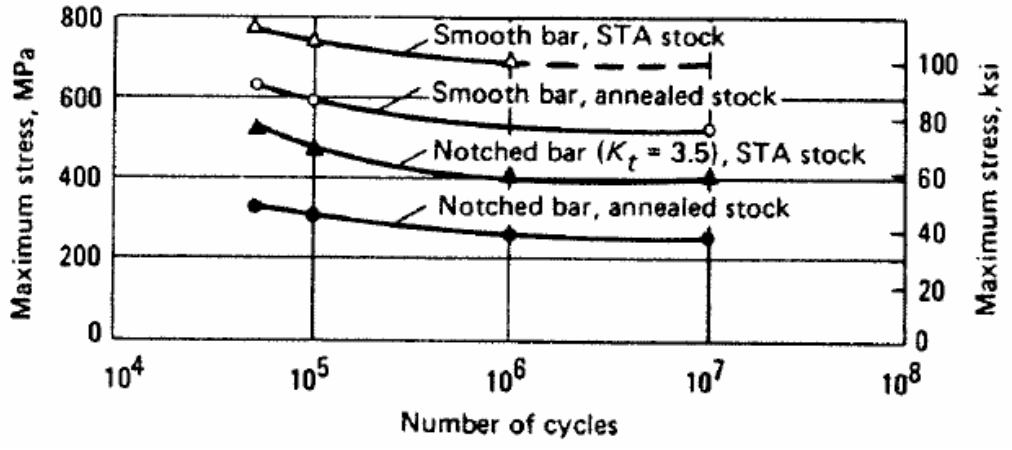

Figure 2. S-N curves of annealed, unannealed, notched, and smooth Ti-6Al-4V. Our as-received samples are annealed smooth bars corresponding to the second graph from the top [18].

2.2 Titanium and its alloys

Ti-based alloys have been widely used in biomedical, aerospace, and many other applications in industry for many decades. Depending on application and required properties, titanium can be employed in pure form or in its alloys forms. This thesis focuses on two main Ti-based metals broadly used in biomedical application namely commercially pure titanium (CP Ti) and Ti-6Al-4V.

2.2.1 Commercially Pure Titanium

Commercially pure titanium (CP Ti) displays an alpha phase allotropic structure, i.e. it exists in more than one crystallographic form [16]. CP Ti is used in medical devices such as cardiovascular stent, lead wires, artificial joints, artificial valve, bone fixation and spinal/trauma fixation devices (plate, screw, pin) [11][13]. Chemical composition of commercially pure grade 2 titanium in %wt is as follows: 99.2Ti, maximum content of 0.25O, 0.03N, 0.015H, 0.3Fe, and 0.1C.

Low content of iron (Fe) in CP Ti diminishes the possibility of having undesired interaction of the metal with the human body. However, CP Ti does not satisfy the strength requirements of all implants, prostheses, and other biomedical devices. Therefore, the need of enhancing the strength of CP Ti has called for different solutions. Developing particular manufacturing processes can help increasing the strength of the metal. For instance, equal channel angular pressing is one of the methods which can provide ultra-fine grain structure, and can increase the fatigue strength of CP Ti as well as the yield and ultimate tensile strength [11]. Creating ultrafine grain structure also showed to enhance cell adhesion (figure 3) [19]. The reason is that in ultrafine grain structure the higher number of grain boundaries contributes to positively affect cell activities, resulting in an improved cell adhesion. Rack and Qazi illustrated fatigue life enhancement as

well as cell adhesion improvement resulting from a fined grain microstructure (figure 3 and figure 4) [11].

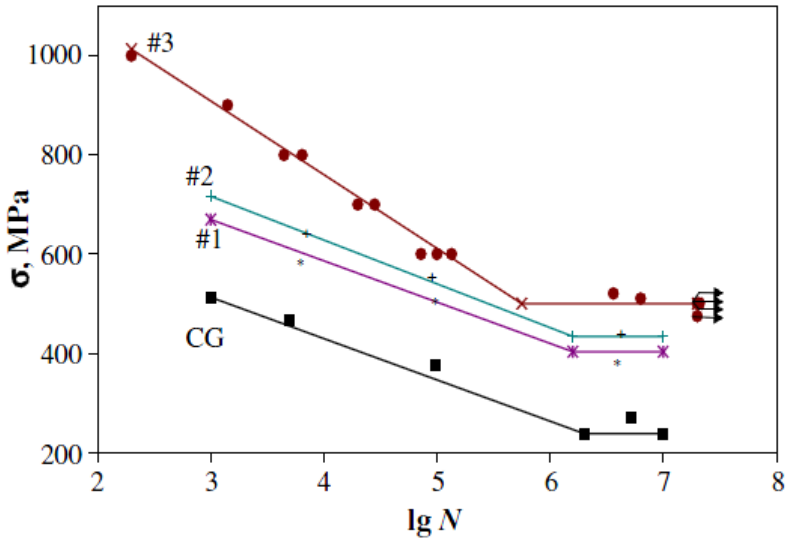

Figure 3. Improved fatigue resistance by creating ultra-fine grained CP Ti grade 2, (CG) coarse grained, (#1) equiaxed cellular, (#2)elongated, (#3) sub-grain microstructure [11].

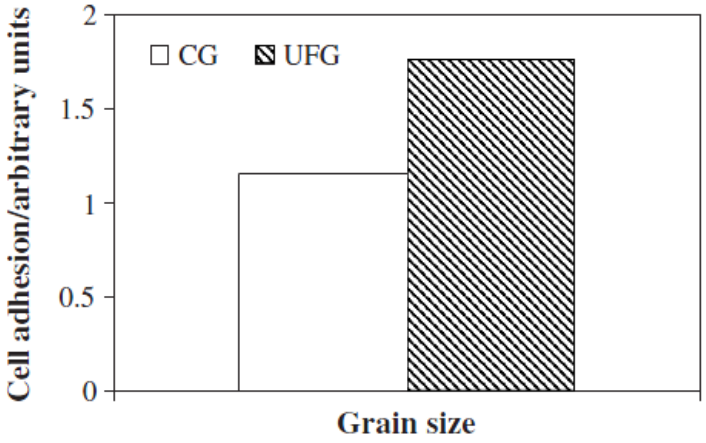

Figure 4. Enhanced osteoblast adhesion on in ultra-fine grained microstructure (UFG), compared to conventional grained microstructure (CG) [11].

However, one of the most widely used ways for enhancing the strength of CP Ti is alloying the metal. This has opened a wide area to researchers to investigate the effects, advantages, and disadvantages of various titanium alloys.

2.2.2 Titanium alloy Ti-6Al-4V

One of the most vastly used Ti-based metals in biomedical applications is Ti-6Al-4V [7]. Small quantities of aluminum and vanadium have a great effect on strength enhancement of CP Ti. As a result, Ti-6Al-4V has been used in applications where the metal is exposed to high stress-bearing situations such as hip prostheses and artificial knee joints [7]. Chemical composition of Ti-6Al-4V in %wt is as follows: 90Ti, 6Al, 4V, maximum content of 0.2O, 0.25Fe.

Endurance limit and ultimate tensile strength of Ti-6Al-4V are almost more than twice as much that of CP Ti. In table 2, different properties of Ti-6Al-4V and CP Ti are displayed. Microstructural difference between CP Ti and Ti-6Al-4V will be studied in section 2.4.1.

2.3 Fatigue failure

Fatigue failure occurs in materials subjected to dynamic and cyclic loadings [20]. Fatigue failure and wear are considered as some of the main failure types of the medical devices (e.g. orthopedic implants subjected to high fluctuating loads) [6]. Figure 5 displays fatigue failure examples in biomedical applications.

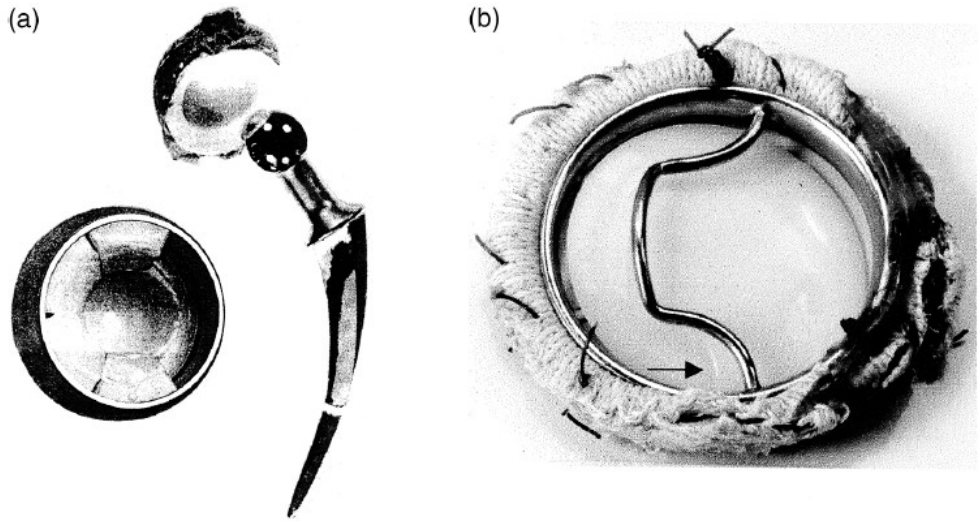

Figure 5. (a) Fatigue failure in hip prosthesis where the crack can be seen in the stent, (b) Small crack (indicated by an arrow) created by fatigue cyclic loading in mechanical heart valve [6].

Fatigue failure evaluation of materials is generally carried out in three ways [6]:

- Stress-life approach (based on S-N curves)
- Fracture mechanics approach
- Corrosion-fatigue

In the first approach, the material is subjected to cyclic loading. The initiation and propagation of cracks as well as their effects on fatigue life and failure can be investigated in detail [6]. This approach and the concept of stress-life curves will be presented in section 2.3.1. In the second method, the fatigue crack propagation of the material is examined in two ways. If the crack is longer than 3 mm, it will be analyzed by compact tension specimen. Conversely, for smaller (1-250 μm) cracks, servo hydraulic machines will be exploited [6]. This method and theoretical concept of fatigue failure analyses are presented in detail in section 2.3.2.

In the third approach, which is extensively used in biomedical applications, the experiment is carried out in the simulated physiological media, and the biomaterial is exposed to corrosion-

fatigue failure. Corrosion-fatigue failure will be studied in depth in the section 2.7.3 where effect of environment on the fatigue life of titanium will be covered.

2.3.1 S-N curves

Utilizing stress versus number of cycles to failure (S-N) curves empirical quantification of the fatigue process could be studied prior to studying the microstructure of the material [21]. In other words, studying the fatigue behavior of the material through its S-N curve is the first step in fatigue failure analysis. Fatigue life, in cycles to failure, can be predicted using the stress-life curve obtained from the fatigue test. Constant cyclic stress amplitude (S) versus number of cycles to failure (N) are drawn on vertical and horizontal axis of the S-N curve respectively. Each material has a characteristic stress-life curve. Some materials such as titanium and steel have an endurance limit (σ_e); i.e. the stress below which fatigue failure would not occur regardless of the number of cycles. Materials such as aluminum and copper do not exhibit an endurance limit. It is therefore obvious that the endurance limit is a crucial parameter in designing components. A typical S-N curve for steel and aluminum is shown figure 6.

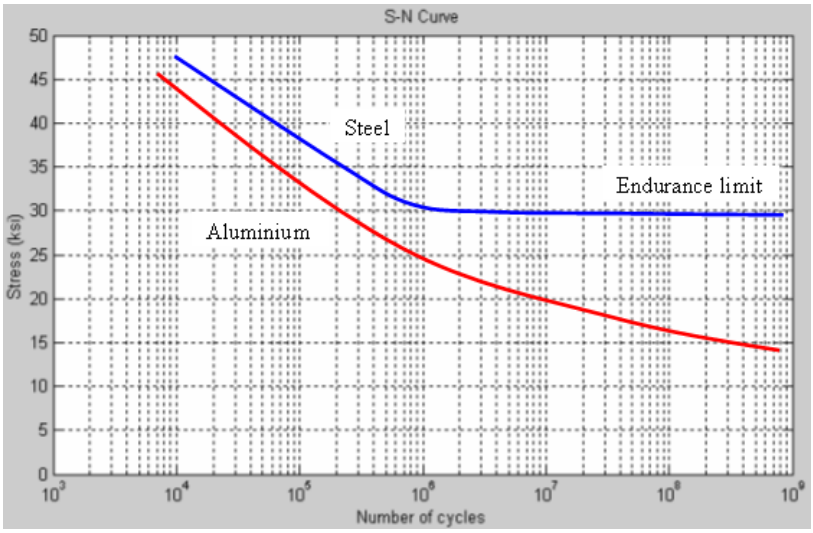

Figure 6. S-N curve of steel that has endurance limit and aluminum that does not [22].

Mean stress, stress range, stress amplitude, and load, elements demonstrated in figure 7, are defined as follows:

$$Stress\ range\ (alternating\ stress, \sigma_{alt}): \Delta\sigma = \sigma_{max} - \sigma_{min}$$

$$Stress\ amplitude: \sigma_a = 1/2(\sigma_{max} - \sigma_{min})$$

$$Mean\ stress: \sigma_m = 1/2(\sigma_{max} + \sigma_{min})$$

$$Load\ ratio: R = \frac{\sigma_{min}}{\sigma_{max}}$$

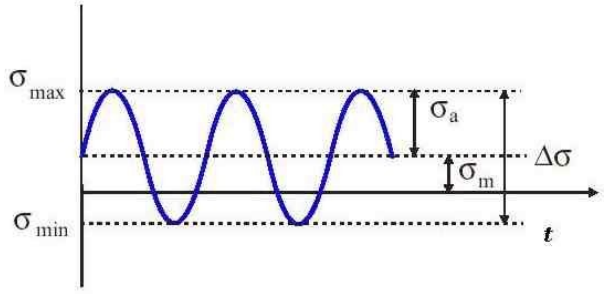

Figure 7. Stress history during cyclic loading [23].

It is generally not possible, due to machines' components inertia and specimen's heat raise, to run the fatigue test at a rate higher that 10 Hz [21]. Significant numbers of tests have to be

performed to form a S-N curve corresponding to each reversible loading case and it is not possible to perform such a curve for each set of alternating and mean stress. One of the methods used to solve this problem is using a Goodman diagram [21]. In this diagram (figure 8) the alternating and mean stresses are constructing vertical and horizontal axes, respectively. A straight line, called lifetime line, connects the endurance limit σ_e on the σ_{alt} axis to the ultimate tensile stress σ_f on the σ_m axis. For any given value of σ_m corresponding value of endurance limit σ_e can be read as the ordinate of the lifeline at that value of σ_m.

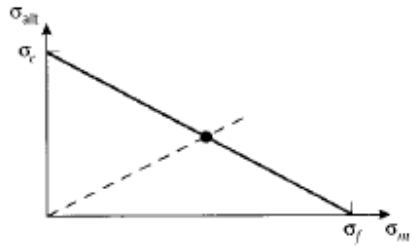

Figure 8. The Goodman diagram [21].

2.3.2 Experimental and theoretical fatigue

Wöhler was the first who performed the systematic experimental studies of fatigue. However, the widely used S-N curves that show the cycles to failure of materials were not developed by him, but by Spangenberg [24]. Wöhler rather summarized these results in tables. In the early 20th century, most of the fatigue studies were conducted in empirical and experimental manner, but still some theoretical concepts were considered [24]. Among the first theoretical concept which dates back to 1910, is the one attributed to Basquin who found the logarithmic relationship between number of cycles to failure and stress amplitude as [24]:

$$\frac{\Delta\sigma}{2} = \sigma_f' \left(2N_f\right)^b$$

Where σ_f' , and b are coefficient and exponent of fatigue strength respectively.

The variation of the amplitude during fatigue life needed to be considered as well. To this end, the hypothesis of the linear damage accumulation, which can be used in prediction of service life of different mechanical components, was established that is called Miner's law.

$$\sum_i \frac{N_i}{N_{fi}} = 1.0$$

Where N_i is number of cycles at a certain stress amplitude and N_{fi} is respective number of cycles to failure.

Researchers focused more on plastic deformation and crack propagation in fatigue failure. The relationship between the number of cycles to failure N_f and the plastic strain $\frac{\Delta\varepsilon_{pl}}{2}$ were introduced as follows:

$$\frac{\Delta\varepsilon_{pl}}{2} = \varepsilon_f'(2N_f)^c$$

Where ε_f' is ductility coefficient and c is the exponent of fatigue ductility.

Later in early sixties, Paul C. Paris used the concept of stress intensity factor that was introduced by Irwin to show that a material subjected to fatigue can always have defects growing at the rate of $\frac{da}{dN}$; i.e. crack growth rate. Irwin found that the stress intensity factor K is related to the geometry of the material through the relationship $K = \sigma\sqrt{\pi a}Y$ where a is the crack length and Y is a geometry function [24].

Paris equation is written as follows:

$$\frac{da}{dN} = C\Delta K^n$$

Where $\Delta K$is the local stress intensity range, and C and n are material specific constants.

The fatigue crack growth rate can be seen in figure 9.

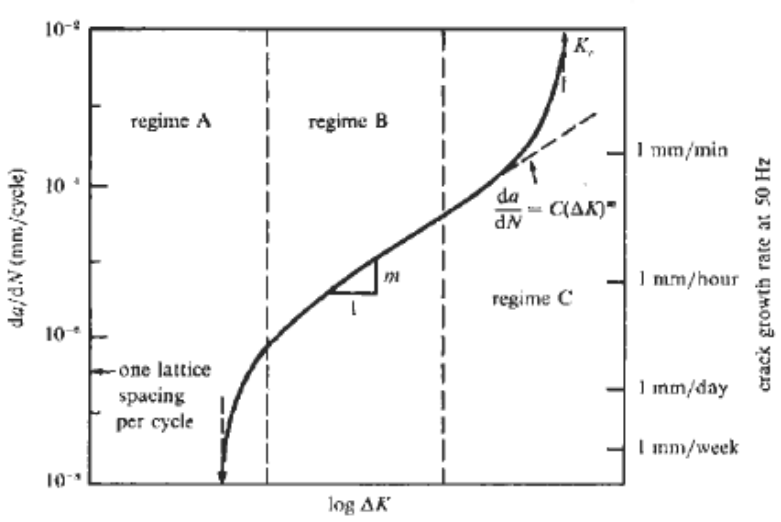

Figure 9. The Paris law for the fatigue crack growth rate [25].

Table 3 illustrates various characteristics of three regimes of fatigue crack growth rate.

Table 3. Three regimes of fatigue crack growth rate based on above Paris diagram [25].

Regime	A	B	C
Terminology	Slow-growth rate	Mid-growth rate	High-growth rate
Microscopic failure mode	Single shear	Striations	Additional static modes
Fracture surface features	Faceted and serrated	Planar and ripples	Additional cleavage and microvoid coalescence
Crack closure levels	High	Low	-
Microstructural effects	Large	Small	Large
Load ratio effects	Large	Small	Large
Environmental effects	Large	Large	Small

The Paris equation is generally used for lifetime prediction of materials. The stress intensity factor from the above equation can be found using the following equation [24].

$$\Delta K = Y(\Delta\sigma)(\pi a)^{1/2}$$

Replacing stress intensity factor ΔK in Paris equation, one may obtain

$$\frac{da}{dN} = C(Y(\Delta\sigma)(\pi a)^{\frac{1}{2}})^n$$

The result of integrating of the above equation will be the total number of cycles to failure, that is

$$\int_0^{N_f} dN = \int_{a_i}^{a_f} \frac{da}{YC(\Delta\sigma)^m \pi^{m/2} a^{m/2}}$$

By performing a fracture toughness test and using the equation $K_{IC} = Y\sigma\sqrt{\pi a_f}$, a_f can be found.

A typical fracture surface of a fatigued specimen consists of two main regions. The first is the section where the crack initiated and propagated slowly and the second region is where the fast and final fracture has occurred. The region of slow crack growth forms clamshell type features with concentric beachmarks. Each beachmark may contain hundreds of striations. Figures 10 and figure 11 are displaying examples of fatigue failure, crack initiation and propagation, beachmarks, striations, and region of final fracture.

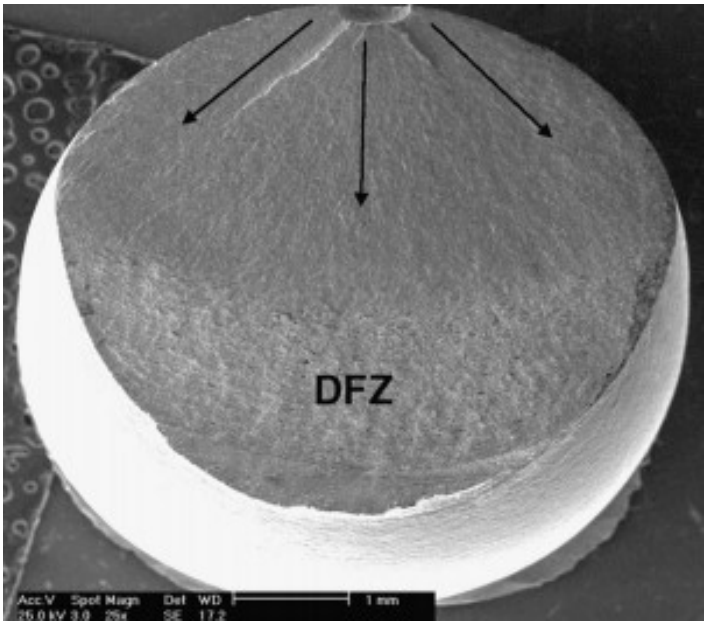

Figure 10. Fatigue fracture surface. Crack initiation started at top then propagated towards bottom of the cross sectional area of the material as the arrows show, and final fracture occurs at ductile fracture zone (DFZ) [26].

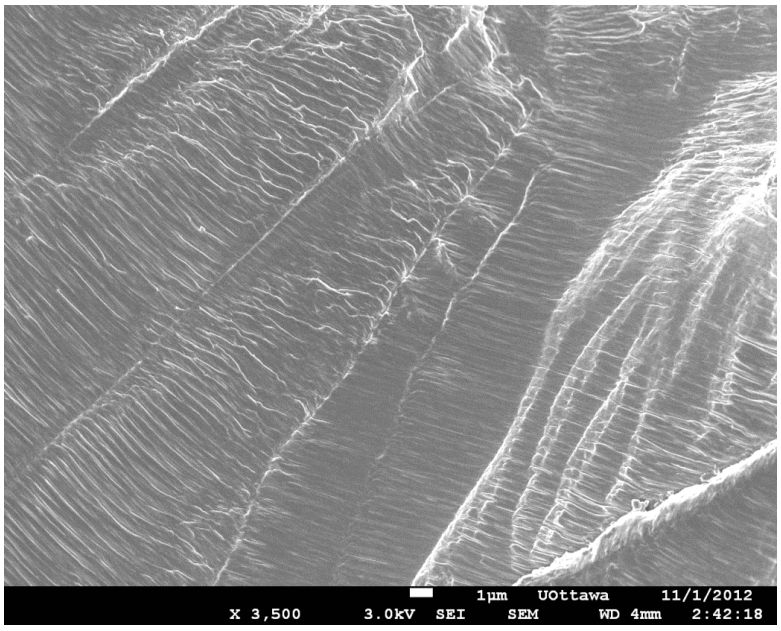

Figure 11. CP Ti beachmarks and striations.

2.4 Effect of surface morphology on fatigue life of titanium

2.4.1 Effect of Titanium microstructure on fatigue crack initiation and propagation

As mentioned earlier, titanium is an allotropic material. At room temperature it has an HCP structure, which is called α phase titanium, and above 882˚C transforms to BCC structure that is α+β phase alloy. The properties of α titanium alloys depend on oxygen content, grain size, texture, and microstructure [17]. Although the microstructure of titanium alloys can be categorized into four types of alpha, near- alpha, alpha-beta, and beta, considering the commercial point of view, they can be grouped as following [17]:

- Unalloyed (CP)
- Alpha and near-alpha
- Alpha-beta
- Metastable beta

Alpha and near alpha alloys are the weakest among all four types. However, they show the best corrosion resistance properties [17]. The difference between various grades of CP Ti comes from content variation of oxygen and iron that are used for different applications. By adding small amount of beta stabilizers to alpha alloys, near-alpha alloys can be formed [17]. Alpha-beta alloys are formed when one or two alpha stabilizers such as aluminum and one or two beta stabilizers such as vanadium or molybdenum are added to titanium [17]. The transformation temperature from alpha-beta or alpha to all beta is called beta transus temperature [17]. Beta transus line consideration is very crucial in heat treatments and in obtaining the desired microstructure of the material.

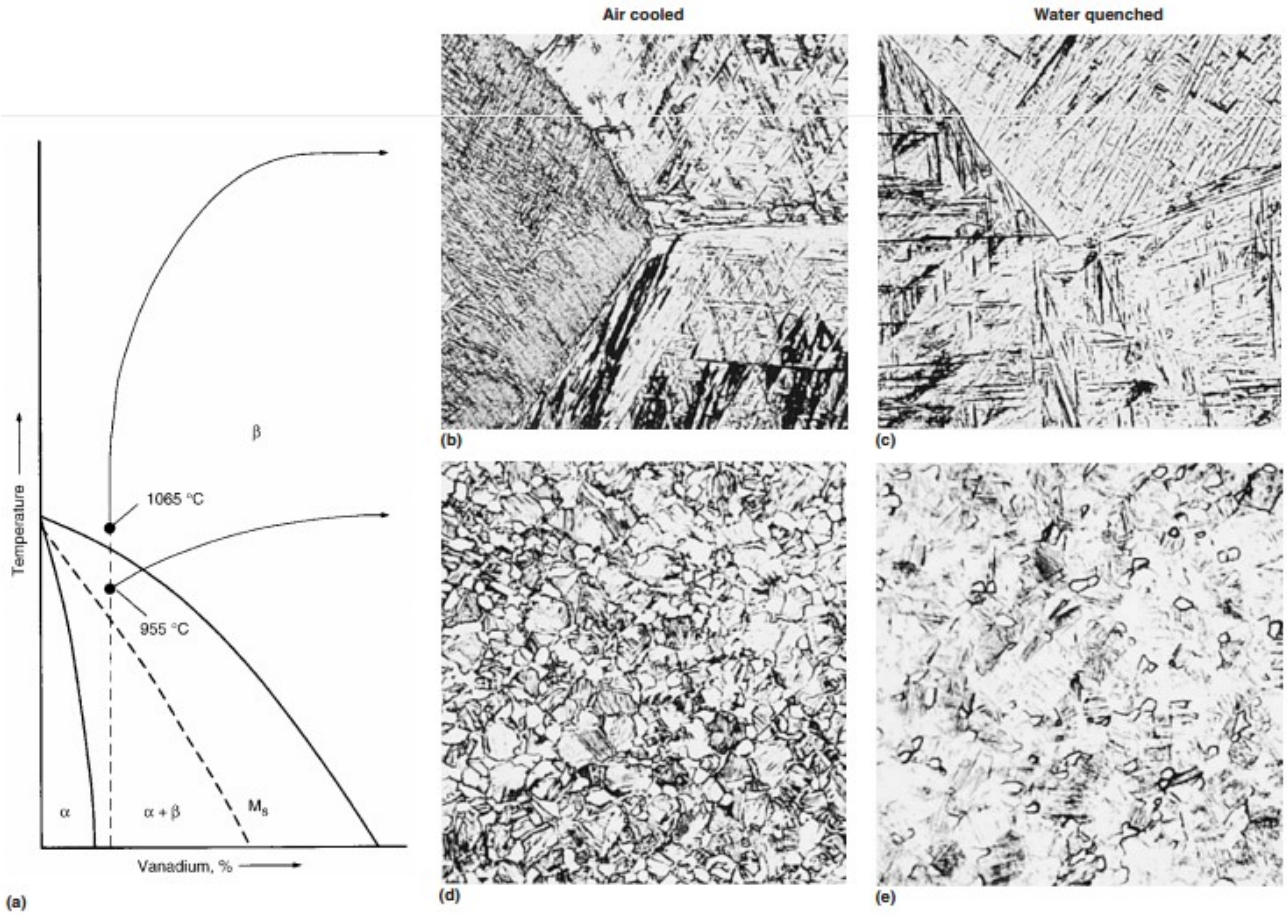

Figure 12. Phase diagram and microstructure of annealed alpha-beta Ti-6Al-4V after cooling, (a) diagram with Ti-6Al-4V indicated, (b) Acicular alpha with prior beta grain boundaries, (c) Alpha prime with beta and prior beta grain boundaries, (d) Grains of primary alpha in a matrix of transformed beta, (e) Equiaxed alpha in a matrix of alpha prime [17].

Fatigue resistance of Ti-based alloys is highly influenced by the microstructure of the material [17]. In the following section different microstructures of Ti-6Al-4V and their effect on the fatigue behavior are studied. In general, fine microstructures tend to delay crack nucleation and on the contrary, coarse microstructure is more resistant to crack propagation [27]. In Ti-6Al-4V alloy, heat treatment below the beta transus line leads to an equiaxed structure, and above this line it results in Widmanstätten pattern [27]. You can see the result of these heat treatments on the microstructure of Ti-6Al-4V in figure 13.

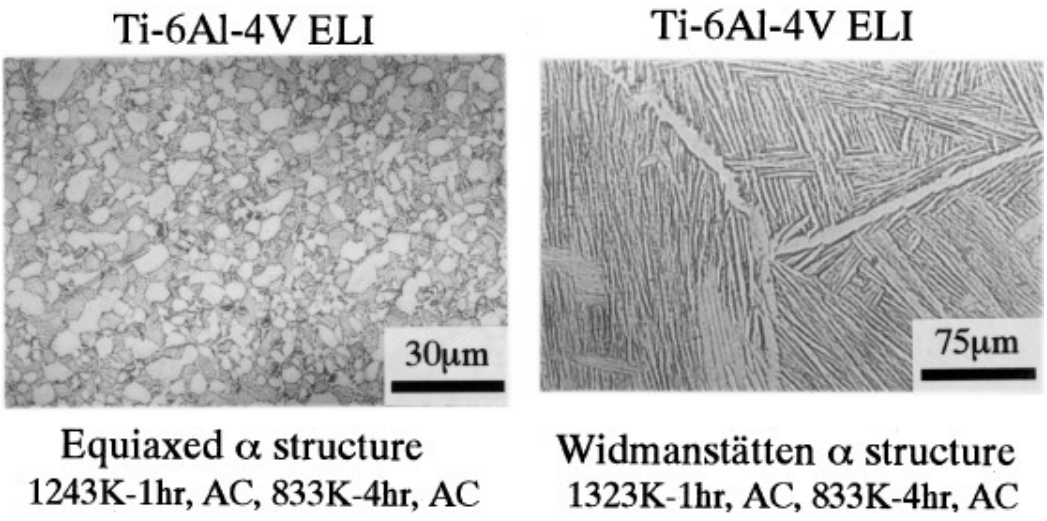

Figure 13. Microstructure of Ti-6Al-4V subjected to different heat treatments [27].

Akahori *et al.* showed through following S-N curve that for Ti-6Al-4V and Ti-6Al-7Nb with an equiaxed structure the fatigue strength is between 700 MPa to 900 MPa, while this value for Widmanstätten structure lies between 550 MPa to 660 MPa [27].

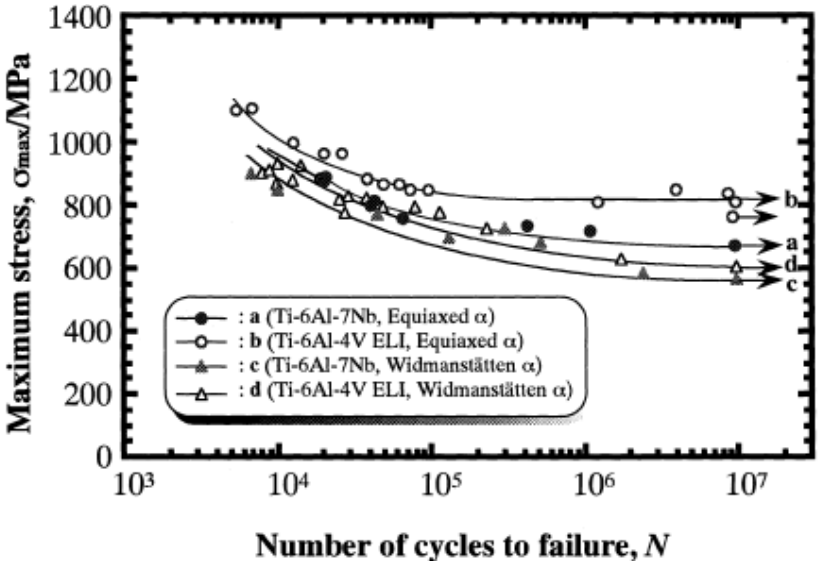

Figure 14. S-N curves of Ti-6Al-4V with equiaxed and Widmanstätten microstructure [27].

The higher fatigue resistance in an equiaxed structure compared to a Widmanstätten structure is attributed to smaller size of the grains that create more barriers to slip and ceases dislocation movements. The difference between the fatigue strength of the Ti-6Al-4V and Ti-6Al-7Nb can be ascribed to the chemical composition of these two titanium alloys.

Akahori *et al.* also stated that crack initiation and propagation resistance is higher in equiaxed α structure than in α Widmanstätten pattern as well as fatigue resistance, which can be ascribed to the reasons mentioned above. In addition, in equiaxed structures the crack initiates at primary α grain boundaries, while its propagation mainly happens between the primary α and β phases [27].

2.4.2 Surface roughness and polishing effects on fatigue performance of titanium

Around 90% of failures of devices in service are due to mechanical causes started at the surface of the material [28]. Rougher surfaces have more stress concentration sites. These are the potential sites for crack nucleation. The created cracks will propagate and finally lead to fatigue failure in the material. Hence, fatigue failure rates are expected to be higher in materials with higher surface roughness (except when the created surface roughness is inducing compressive residual stresses such as surface roughness created by sandblasting and other similar methods). However, to improve bone integration a higher surface roughness (compared to smooth samples) is required to stimulate cell activities [29]. Therefore, optimizing the surface topography and roughness of the Ti-based metals to integrate biocompatibility and fatigue resistance is critical. Various methods are used to decrease surface roughness and get a better surface finish towards obtaining a better fatigue resistant material. In the following section the effects of conventional and electrolytic polishing of CP Ti and Ti-6Al-4V on fatigue life will be investigated. Aside from carrying out tests in air, fatigue tests have also been performed in fluoridated artificial

saliva to simulate the biological environment. A. S. Guilherme *et al.* stated that electrolytic polishing results in lower surface roughness than conventional polishing [28]. It is also shown that for both of CP Ti and Ti-6Al-4V polishing did not have any significant influence on fatigue strength of the material. However, it was found that the biological environment had a great effect on fatigue life. This effect was much greater in CP Ti than in Ti-6Al-4V [28]. The influence of the environment on fatigue life of the materials will be discussed in section 2.7.3. It is worth noticing that the scale of the surface roughness plays a vital role in fatigue life of materials. Guilherme *et al.* did not find a significant influence on the fatigue performance of CP Ti and Ti-6Al-4V after decreasing their surface roughness by polishing [28]. However, it should be taken into account that the mean surface roughness in their experiment was 0.31 μm for CP Ti, and 0.25 μm for Ti-6Al-4V [28].

Table 4. Mean values (SDs) of surface roughness (μm) for CP Ti and Ti-6Al-4V [28].

	Polishing	**Protocols**	
Metal	Conventional	Electrolytic	Mean value
CP Ti	0.35 (0.05)	0.27 (0.06)	0.31 (0.05) a
Ti-6Al-4V	0.28 (0.08)	0.21 (0.04)	0.25 (0.06) b
Mean value	0.32 (0.06) A	0.24 (0.05) B	

2.5 Surface science and biology

The biomaterial-host tissue interactions during the application of a cyclic load provoke changes on various scales. Deformation of an implanted biomaterial has repercussions on the surface molecular absorbed layer, oxide film, and inner deformed layer as displayed in figure 15 [6]. The interaction of these elements with the surrounding tissues will ultimately determine the overall biological response to an implanted biomaterial.

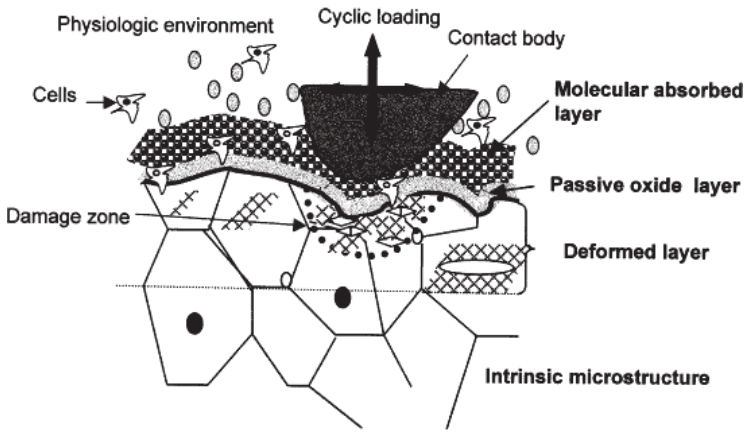

Figure 15. Schematic of the deformed biomaterial in the physiological environment [6].

As stated in section 1.1, various surface treatments have been employed to create surface features on the surface of the biomaterial to promote and stimulate cellular activities. These surface features will only be effective and beneficial if they are recognized by the biological system, the so-called biorecognition [30]. In this context, the biocompatibility of biomaterials (i.e. capacity to integrate in tissues without causing allergic or inflammatory response) is tightly connected to cell adhesion, the first phase of cell colonization. The quality of this initial step will affect the following tissue integration and bone formation [31].

2.6 Surface modification techniques

2.6.1 Nanoscale surface modifications of metallic surfaces

The surfaces of biomaterials can be modified by different techniques at various scales. Several studies have shown that the most effective treatments are generally those which impact the surface properties at the micrometric and nanometric scales. Some of the most widely used surface treatments employed are polishing, blasting, shot peening, and plasma spraying [28][29][32][33]. These methods, used individually or in combination with other surface treatments, create inhomogeneous surface topographies at the micrometric scale. They also (see

section 2.6.4) have demonstrated to improve the osseointegration and impact the cellular activities [34]. However, most of the cells activities are carried out at the nanoscale, and therefore surface micrometric features are too coarse to directly impact cellular functions. Nanometric features have demonstrated to be more effective in influencing the cellular activities, since they act at the scale at which cells function, namely the nanoscale. These nanometric cues have the ability to control the interactions between biomaterials and the host tissue, and therefore, techniques capable of creating such features have attracted increasingly more attention and found more applications in recent years [35][36].

It is noteworthy mentioning that although the fundamental interactions occur at the nanoscale, there is an intrinsic connection between the nanometer and the micrometer length scales in cellular processes [30].

2.6.2 Anodization

Commercially pure titanium and titanium alloys are currently exploited because of their combined excellent biocompatibility, mechanical properties, and corrosion resistance. Excellent biocompatibility and corrosion resistance of Ti-based metals are attributed to the spontaneous formation of a protective oxide layer on the surface of the material [37]. Pristine titania (titanium dioxide, TiO_2) exhibits a thickness ranging from 2 to 10 nm [8][38].

Considering that this surface oxide layer is responsible for the excellent biocompatibility and corrosion resistance of the Ti-based metals, many methods have been employed to increase its thickness and alter its topographical and physicochemical properties. One of these effective techniques for nanostructuring the surface of titanium-based metals is anodic oxidation, often called anodization. Anodization is a process in which the titanium acts as anode electrode of an electrolytic cell. Depending on electrochemical process parameters such as voltage, electrolyte

type and concentration, current density and time, arrays of nanotubes with different diameters and lengths can be fabricated. For instance, anodizing titanium in HF (hydrofluoric acid) electrolyte for less than two hours at an applied potential of 20V yielded the formation of nanotubes with a diameter ranging between 70 and 100 nm [39][40]. The thickness of 250 nm was obtained by anodizing titanium in 0.5% HF electrolyte at 20V for 30 minutes [41]. The schematic of the process of nanotube fabrication can be seen in the figure 16.

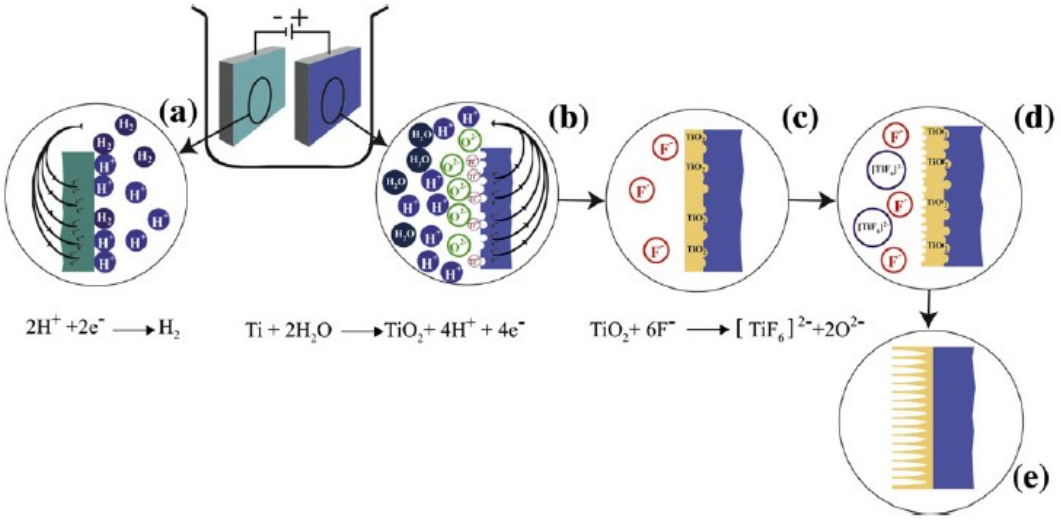

Figure 16. TiO_2 nanotube fabrication. (a) cathodic reaction, (b) anodic reaction, (c) transition state of TiO_2, (d) onset of nanotube formation, and (e) mature titania nanotubes [38].

Crawford and Chawla developed a dual TiO_2 structure by superimposing nanotubes (with diameter ~ 50 nm) on a rough surface of a titanium implant (roughness of ~ 1-20 μm) [41]. This hierarchical structure is believed to improve the biocompatibility of the metal since it combines both the nanostructure, which enhances the cell-implant interaction activities, and microfeature, which improves the interlocking and bone fixation of the implant [38].

Titania nanotubes, created on Ti-based metals with anodization have shown to enhance bone cell growth [42]. Popat *et al.* investigated cell adhesion and proliferation onto titania nanotubes and compared the results to those of smooth titanium and polystyrene [42]. The number of cells

present on the surface of the nanotubular titania surfaces was 40% higher as compared to smooth titania surfaces (figure 17).

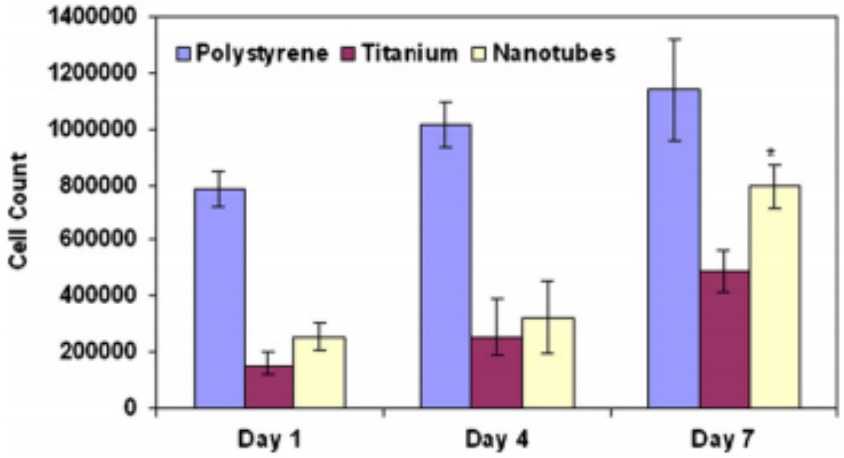

Figure 17. Nanotubular surfaces show 40% higher cell proliferation after 7 days of cell culture compared to titanium surfaces [42].

2.6.3 Oxidative nanopatterning in Piranha solution

Oxidative nanopatterning is another technique for nanostructuring titanium-based metals. This process is carried out by immersing the metal in Piranha solution (i.e. a mixture of sulfuric acid, H_2SO_4, and hydrogen peroxide, H_2O_2) at different concentrations and various time intervals. The aim of this process is to remove the native oxide layer from the surface of titanium and recreate this layer under controlled conditions, in ways to engender new features capable of stimulating cellular activities at the nanoscale and enhancing the osseointegration [43]. The rationale behind this technique is that a combination of a strong acid and an oxidative agent has shown to create a sponge-like structure of nanosized pits on the surface, which confers new biological functionalities to the metal [43]. Yi *et al.* treated CP Ti samples in the Piranha solution (50:50 mixture) at 22 ˚C for 2 hours, and found that the diameter of the nanopores and the thickness of the formed oxide layer were respectively 20-22 nm and ~ 32-40 nm [43]. In a similar

experiment, Variola *et al.* exploited the same solution on Ti-6Al-4V revealing that the diameter of nanopits ranged from 13 to 21 nm and the thickness of the oxide layer from 15 to 45 nm [44]. The nanofeatures created by this simple yet very effective etching technique are notably influencing the early steps of *in vitro* osteogenesis [43]. De Oliviera *et al* demonstrated in fact that the nanoporous surfaces enhance the formation of bone-like nodules, an evidence of the enhanced mineralization of bone cells (figure 18) [45].

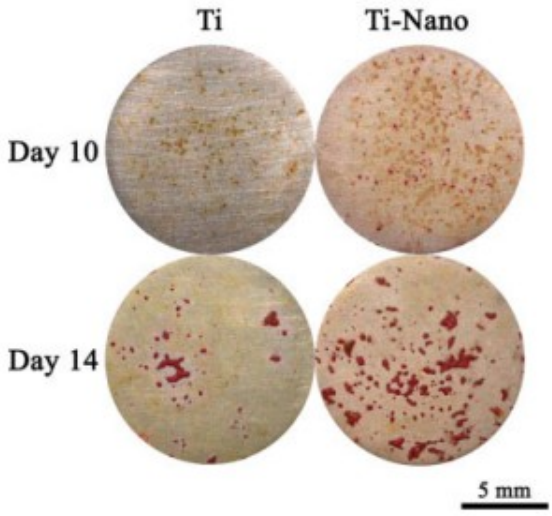

Figure 18. Comparative red staining of 14-day old osteogenic cell culture grown on polished Ti (left) and treated Ti with piranha solution [45].

Richert *et al.* showed a similar enhancement of cell growth on the surface of the Ti-6Al-4V [46].

2.6.4 Microscale modification techniques

In this section, selected commonly used microscale modification techniques will be briefly presented. Shot peening is a cold working process that improves the mechanical properties of the material by introducing compressive residual stresses on its surface.

Similar to shot peening, grit blasting and sandblasting are processes in which the material is bombarded by particles to produce surface features. Small ceramic particles such as alumina, titanium oxide, or calcium phosphate are projected through a nozzle with high velocity onto the material's surface. These methods improve the osseointegration and enhance bone-implant interlocking [47].

Another category of surface modification techniques includes processes which deposit a coating on the surface of the material. Plasma spraying, cold spray deposition, detonation gun spraying, and similar spraying techniques are mechanisms used in order to deposit a coating on the surface of the material. Various kinds of powders and particles are employed in these techniques. For biomedical applications, coatings consisting of titanium and hydroxyapatite particles are mostly used to coat the surface of the implants [47]. Titanium plasma spraying is found to improve the bone-implant interlocking and adhesion between the material and body [47]. Since the biocompatibility of pure titanium is higher than that of Ti-6Al-4V, and Ti-6Al-4V has higher yield and endurance limit, CP Ti particles can be used to coat the surface of Ti-6Al-4V [47]. Hydroxyapatite (HA) is also used to coat the bulk material for enhancing osseointegration [32]. Hydroxyapatite (HA) with chemical formula of $Ca_5(PO_4)_3(OH)$ is a member of apatite family, a family of phosphate minerals [48]. It is one of the main components of bone mineral and widely used in biomedical applications due to its excellent bioactive properties and high ability to create strong chemical bonds with natural bone [49][50]. This surface layer accelerates the rate of osseointegration, since the existence of calcium phosphate in HA helps the healing process and improves cell attachment and bone in-growth [47]. Another type of coating is based on the deposition of WC-10%Co-4%Cr on Ti-6Al-4V, which showed to improve its biocompatibility [51]. Surface characterization of biomedical implants has always attracted the attention of

scientists. Different methods have been utilized to achieve a close to ideal biocompatible implant. Cook *et al.* performed a research and studied the fatigue behavior of some of these treatments that improve implant fixation [15]. They compared the results of porous coating, heat treatment, and also the notch effect on fatigue life of Ti-6Al-4V. Porous coating applied to the implant to accelerate osseointegration and to improve bone-implant fixation and interlocking. In addition, certain heat treatment is required prior to applying the porous coating in order to obtain adequate level of biocompatibility [15].

2.7 Fatigue behavior of surface modified titanium-based metals

2.7.1 Effect of anodization on fatigue life of titanium

Nanotubular structures created by anodization could act as surface defects and/or stress-raisers. These could therefore be responsible for initiating crack nucleation and ultimately increasing the probability of premature failure under the typical *in vivo* cyclical loads. For this reasons, the potentially adverse effects of surface modifications on the fatigue resistance of anodized titanium have been the focus of previous studies. Leinenbach *et al.* studied the effect of thermal and anodic oxidation on fatigue life of CP Ti and also titanium alloy Ti-6Al-7Nb [8]. Figure 19 illustrates a comparison between S-N curves of polished, thermally oxidized, and anodically oxidized CP Ti presented by C. Leinenbach *et al.* [8].

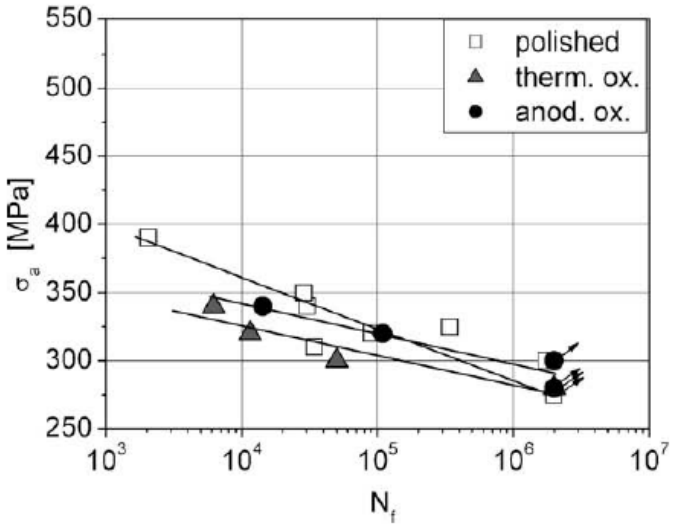

Figure 19. S-N curves for polished, anodically and oxidized CP Ti [8].

Results from this study (figure 19) indicate that there is no significant difference between polished and anodized CP Ti. However, thermally oxidized specimens seem to be characterized by a slightly decrease of the fatigue life. The lower fatigue resistance of thermally oxidized CP Ti is attributed to the structure of the thermal oxide layer, highly crystalline and more brittle [8].

In a similar study, P. Costa *et al.* examined and compared the fatigue behavior of polished and anodized Ti-6Al-4V alloy [10]. They have shown that anodization reduces the alloy's fatigue life. Shot peening prior to the treatment contributes to improve the fatigue resistance and, to a certain extent, compensates the adverse effects of anodization (figure 20) [10].

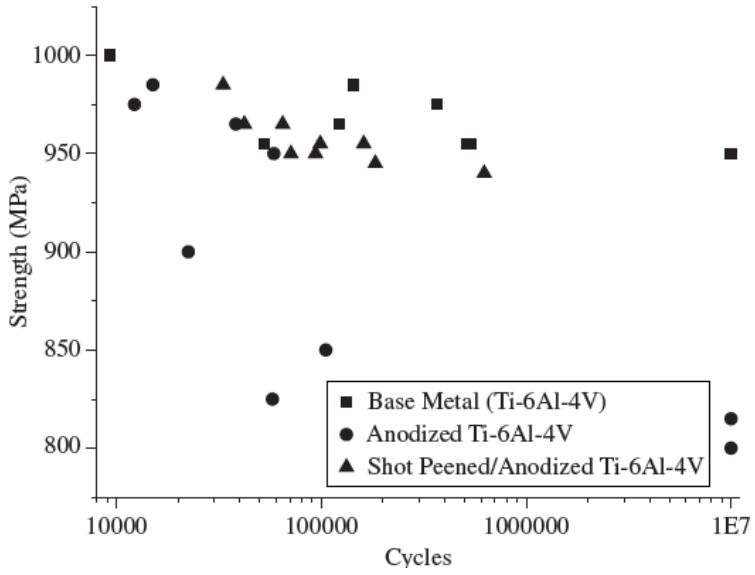

Figure 20. S-N curves for anodized, shot peened/anodized and as-received Ti-6Al-4V [10].

Similarly, Apachitei *et al.* analyzed the behavior of anodized and polished Ti-6Al-4V and Ti-6Al-7Nb alloys [9]. The resulting reduction of the fatigue resistance of both anodized titanium alloys Ti-6Al-4V and Ti-6Al-7Nb is illustrated in figure 21 [9].

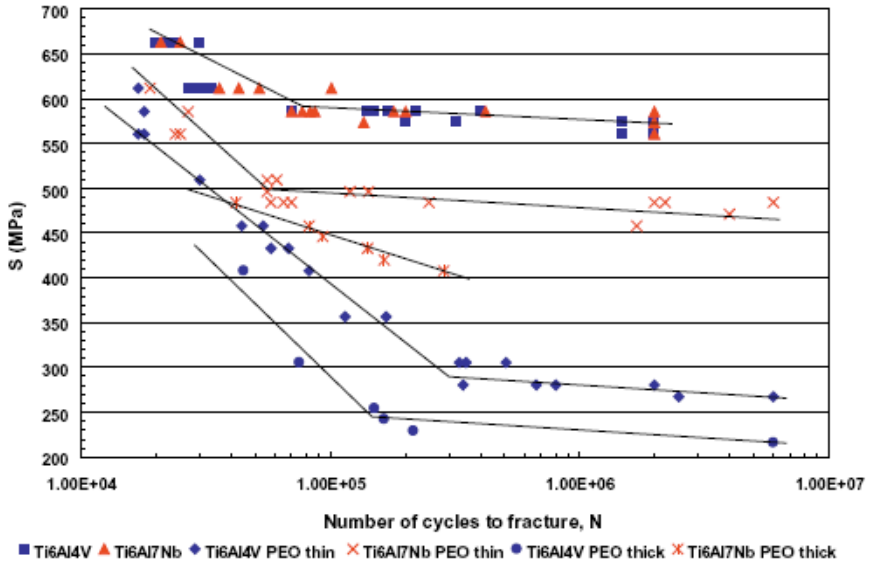

Figure 21. Fatigue behavior of coated and uncoated titanium alloys Ti-6Al-4V and Ti-6Al-7Nb. Anodization decreased the fatigue resistance of the titanium alloys Ti-6Al-4V and Ti-6Al-7Nb [9].

Titanium dioxide may experience structural changes from amorphous to crystalline during anodization process as its thickness is increased [9]. This change in structure can generate a more brittle oxide layer, more susceptible to premature crack initiation, propagation and ultimately failure. Results by Apachitei *et al.* (figure 21) demonstrated that the thickness and brittleness of anodized Ti-6Al-4V increased, leading to a failure at a lower number of cycles under fatigue loads [9].

2.7.2 Influence of other relevant surface modifications on fatigue life of titanium

2.7.2.1 Influence of acid etching on titanium fatigue behavior

Acid etching has been used to create surface features to improve osseointegration. This treatment generates micro pores in size range of 0.5 to 2 μm on titanium implants [47]. Strong acids such as HCl, H_2SO_4, HNO_3, and HF are some of the most widely used chemicals for acid etching. Main parameters that affect the outcome of the treatments and result in desired surface features are the acid concentration, duration of the immersion, and temperature of the solution. Pazos *et al.* investigated the effects of acid etching, blasting, and combination of the both on the fatigue life of CP Ti [52]. Commercially pure titanium was immersed in the 9M sulfuric acid solution at 60˚C for 15 minutes and blasted by Al_2O_3 particles with maximum of 600 μm in size. The three conditions, acid etched (A), blasted (B), and combined acid etched/blasted (BA) were then tested and the results were compared to the as-machined specimens (figure 22).

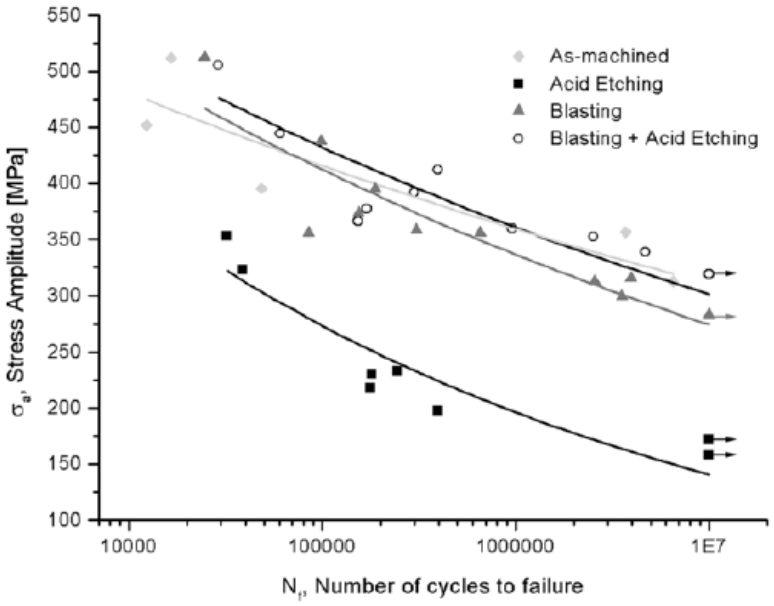

Figure 22. S-N curves of various surface treatments on CP Ti [52].

Blasting and combined blasting and etching of CP Ti suggest a minor impact on fatigue life of the material as compared to the as-machined specimens. On the other hand, acid etching of CP Ti had notable effects and significantly diminished the fatigue resistance. Increased surface roughness due to etching resulted in an increase of stress raisers and consequently enhanced number of cracks nucleation. The surface defects created by sulfuric acid appeared in form of micrometric holes and intergranular corrosion, factors which caused the fatigue failure [52]. The improved fatigue life of the acid etched CP Ti by prior blasting is attributed to the lack of intergranular attack [52]. Pazos *et al.* ascribed the lack of intergranular attacks to plastic deformation of the surface due to blasting which introduced high surface energy and decreased the grain boundary activity, thereby limiting the number of definite grain boundaries for creation of intergranular corrosion [52].

2.7.2.2 Effect of other relevant mechanical surface treatments on the fatigue life of titanium

Many research groups have studied and analyzed the fatigue behavior of titanium-based metals modified by the treatments outlined in section 2.6.4. In order to observe the effects of these treatments on fatigue resistance, S-N curves were recorded and compared. Since the scope of this Thesis is focused on nanoscale surface modifications, detailed analysis of the effects of microscale surface treatments on the fatigue life of Ti-based metals only briefly considered.

By studying the S-N curves (appendix I, figure 56 - figure 60) corresponding to each surface modified Ti-based metal one may find that shot peening and carbon coating are the only processes that are improving the fatigue performance of the metal. Other mentioned surface treatments namely HA and WC-10%Co-4%Cr coating and grit blasting are decreasing the fatigue resistance of the titanium-based metals. Improved fatigue resistance of shot peened samples is ascribed to induced compressive residual stresses and slight increase of endurance limit of carbon coated Ti-6Al-4V is attributed to the enhancement of surface hardness of the metal due to formation of titanium carbides on the surface [15][29]. Grit blasting however decreased the fatigue performance of Ti-6Al-4Vdue to created stress raisers on the surface of material generated by blasting and also the propagation of the cracks nucleated by hard blasting particles. Decreased fatigue lives of HA and WC-10%Co-4%Cr titanium-based metals are ascribed to delaminating of the coating and also introduction of residual stresses during the coating processes[49][50][51].

2.7.3 Effect of the environment on titanium fatigue performance

The environment to which the material is exposed has a great influence on its fatigue behavior. In the biomedical field, orthopedic implants exposed to corrosive physiological environment with high salt concentrations, enzymes, proteins and cells [53]. Studying the effects of cyclic

loading on the material in such a corrosive environment is often called corrosion-fatigue behavior studies. Corrosive-fatigue testing of orthopedic implants is usually performed in simulated body-type fluids such as saline, saliva, and Ringer's or Hanks' solutions [53]. Ringer's and Hank's solutions are salt-based solutions to simulate body-type fluid used for *in vitro* experiments.

In such an environment the fatigue resistance of titanium is found to be decreased to quite high level. R. A. Zavanelli *et al.* performed fatigue tests on titanium alloy Ti-6Al-4V in two different physiological environment conditions and discovered a great decrease in fatigue life of the material as compared to the air condition [53]. Similarly, C. Fleck noticed a reduction in fatigue life of the CP Ti in Ringer's solution when compared to the air [53]. The results of these two experiments can be seen in figure 23 and table 5.

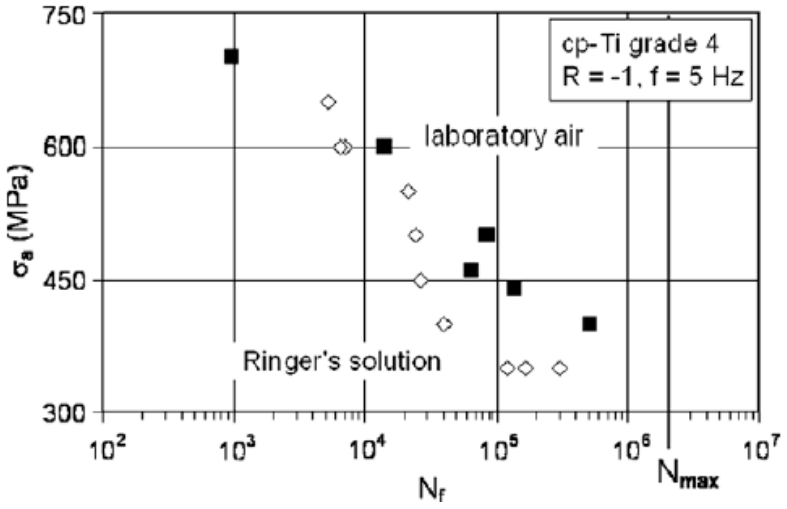

Figure 23. S-N curve corresponding to fatigue behavior of CP Ti in air and Ringer's solution [53].

Table 5. Mean and standard deviation of fatigue life of CP Ti and Ti-6Al-4V in different environents [54].

	In air	Synthetic saliva	Fluoride synthetic saliva
CP Ti	19,157 (SD 3,6240	9,099 (SD 5,655)	5,772 (SD 2,824)
Ti-6Al-4V	21,269 (SD 8,355)	9,469 (SD 2,404)	6,429 (SD 2,346)

The fact that the oxide layer which is spontaneously formed on the surface of the titanium is a good protection against the corrosion is true when the titanium is dealing with static conditions; however when it comes to cyclic loading Lucas and Lemons found out that this layer is not a stable and secure protection against galling and seizing as it is in static conditions [55]. Therefore, the pitting corrosion defects, which many researchers reported their appearance on titanium implants in physiological media that occurred due to the exposure to the corrosive environments [54], act as stress concentrations where the cracks initiated. In addition, titanium is vulnerable to hydrogen embrittlement process and in environments such as physiological media, where the metal is exposed to fluoride solutions, crack propagation is accelerated under the stress [56]. The corrosion behavior of titanium when exposed to fluoride solution is related to HF concentration; if the concentration of HF in the solution exceeds 30 ppm the oxide layer will be demolished [57]. In figure 23 where CP Ti fatigue examined in Ringer's solution, one may notice that corrosion effectiveness gets more pronounced when the material experienced higher cycles toward failure. It is declared that fatigue failure accelerated in higher cycles due to the fact that the repassivation of the mechanically damaged surfaces is hardly occurred in deficiency of enough oxygen [53].

In this context, a future work related to this Thesis will consider the effects of the physiological medium in which test specimens will be immersed.

2.8 Surface characterization techniques

2.8.1 Optical Microscopy (OM)

One of the most widely used microscopy methods to study the surface of the materials is optical microscopy. A typical optical microscope consists of an illuminator, condenser, objective, and eyepiece [58]. In this process, illuminator passes the light through the condenser and the specimen. Some of the light that passes around and through the specimen is undisturbed, which forms the background light and called undeviated light [59]. However, some of the light that passes through and around the specimen is diffracted and deviated. The half wavelength caused by specimen enables the direct light to make destructive interference that both arrive at fixed part of the eyepiece. The eyepiece further magnifies this image and projects it on to the film plane of the camera [59].

To be able to characterize the surface of the material under the optical microscope, specimens require polishing, washing in ultrasonic bath, and sometimes controlled etching. Grain orientations and their sizes, void growth, twin developments, slip bands, and other material science phenomenon could be observed using the optical microscope. Figure 24 demonstrates grain type, orientation, and size for CP Ti. Through this image one may find the microstructure of the material, grain sizes and their orientation, purity, homogeneity, crystal defects, existing phases, voids or cracks, possible twins, and etc.

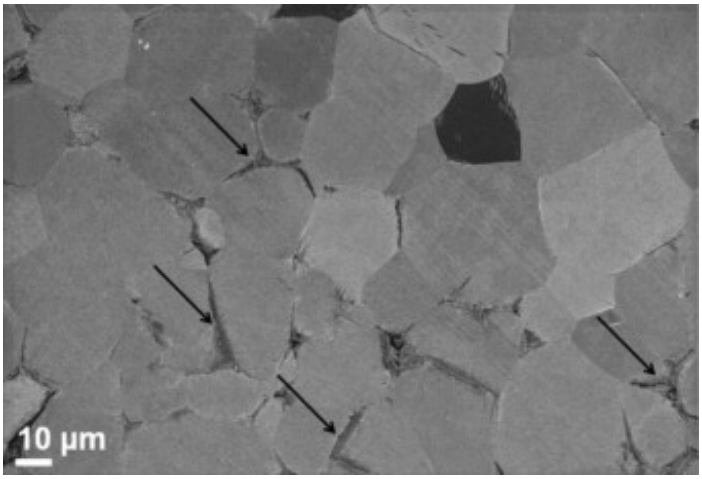

Figure 24. Microstructure of CP Ti, equiaxed alpha grains [60].

2.8.2 Scanning Electron Microscopy (SEM)

Scanning Electron Microscopy (SEM) is a technique that has been used for decades in materials science, and other science fields, to study the surface topography of the materials and obtain high quality images at high magnifications and high spatial resolutions through beams of electron. A scanning electron microscope utilizes a gun to shoot electrons, and two or three electromagnetic lenses to demagnify the electron beam into a probe. Electrons interaction with the specimen creates secondary electrons collected by the suitable detectors and magnified. The outcome is a related map of these collected signals from the scanned area of the specimen. The map produced by the signals carries information about the surface topography and composition of the material. Scanning Electron Microscope used to obtain images from a conductive material; non-conductive materials are coated with a conductive material to get prepared for the observation. Sample preparation for SEM analyses is very crucial, since this device is very sensitive. Any contamination on the surface would be counted as an obstacle for better scanning of the surface, therefore samples have to be well-prepared and washed for imaging. Nanofeatures and

nanocracks on the surface of the materials that are not visible with optical microscopes can be observed using SEM (figure 25).

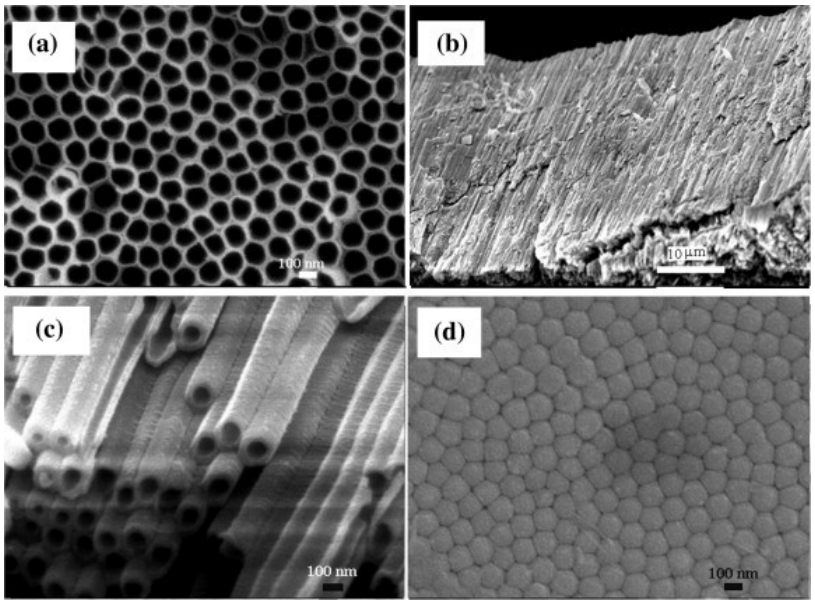

Figure 25. SEM images of TiO_2 nanotubes formed in ethylene glycol + 0.3 wt. % NH4F + 2 vol. % H2O [38].

Chapter 3 Experimental procedure

3.1 Material's characteristics

3.1.1 As-received specifications and mechanical properties

The two metals and total of the three surface treatments have generated six different conditions for analysis (table 6).

Table 6. Six groups of samples from two material types and three treatments.

	Mechanical polishing	Anodization	Oxidative nanopatterning
CP Ti (grade II)	☑	☑	☑
Ti-6Al-4V	☑	☑	☑

Pure titanium has low density and good ductility, and depending on the implant function its strength can be increased by alloying pure metal and obtaining alloys such as Ti-6Al-4V. CP Ti and Ti-6Al-4V were chosen to assess their fatigue resistance when introduced to various surface treatments. The materials are received from Titanium Industries Inc, Montreal, Quebec, Canada. Table 7 presents the specification of each as-received material.

Table 7. Characteristics of the as-received samples received from Titanium Industries Inc.

Material	Size	Chemical composition (%wt)
CP Ti (grade 2)	Wire 0.125"×3'	0.01N, 0.02C, 0.05Fe, 0.1O, 0.003H, rest Ti
Ti-6Al-4V	Wire 0.125"×3'	0.01N, 0.03C, 0.12Fe, 0.13O, 0.011H, 6.2Al, 4.1V, rest Ti

The material properties are presented in table 8.

Table 8. Mechanical properties of the as-received samples.

Material	Grade	Tensile strength (MPa)	Yield strength (MPa)	Modulus of elasticity (GPa)	Endurance limit (MPa)	% Elong.
CP Ti	2	345	275	105	220	20
Ti-6Al-4V	5	895	828	116	510	10

The fatigue strength of CP Ti II, commercially pure titanium grade 2, is 289 MPa at 10^6 cycles and Ti-6Al-4V resists fatigue failure to the same amount of cycles at 510 MPa [12]. The fatigue behavior of CP Ti and Ti-6Al-4V can be observed in figure 1 and figure 2.

3.1.2 Microstructure

As mentioned in sections 2.4.1, the microstructure of the material has a great influence on both its biocompatibility and fatigue resistance. Therefore, the microstructure of the as-received samples had to be examined. For this purpose, samples were first mechanically polished, and then etched with 0.5% hydrofluoric acid (HF). Finally, they were rinsed with distilled water, washed with acetone in an ultrasonic bath, and air dried. The samples were then taken under the optical microscope (OM) to investigate their microstructure.

3.2 Sample preparation

3.2.1 Sample design

The as-received samples were all in rod shape 0.125" in diameter and 3’ long. The design of the samples had to be in a way to meet and satisfy the fatigue testing requirements. To this end, the American Society for Testing and Materials (ASTM) International Standards designation E466-07 Standard, i.e. *Practice for Conducting Force Controlled Constant Amplitude Axial Fatigue Tests of Metallic Materials* was considered. Each standard provided by ASTM International corresponds to certain test conditions [61]. This standard is dedicated to tests where the fatigue strengths of notched and unnotched metallic materials have to be examined axially at constant amplitude in air. Based on this standard, the design of the sample has to be in a way that the failure occurs in the narrowest part of the test section. Choosing the continuous radius type for the circular cross section, in accordance to the ASTM International Standards the radius of curvature should not be less than eight times of the diameter of the test section. In addition, the length of the test section should be at least three times greater than the diameter of the narrow section.

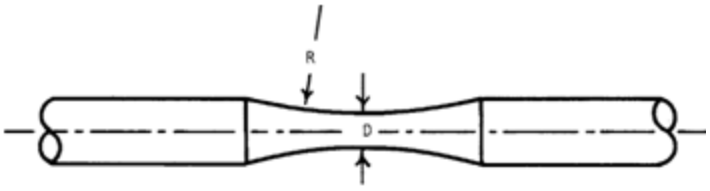

Figure 26. Specimen with continuous radius, ASTM International Standards for axial fatigue resting, designation E466-07 [61].

The diameter of the narrow section of the dog-bone shaped samples had to be found based on the fatigue behavior of the material. In other words, one must ensure that the applied stress to CP Ti and Ti-6Al-4Vfor the fatigue test lies above the endurance limit of the material to provoke failure. Considering that the endurance limit of the Ti-6Al-4V is almost twice that of the CP Ti,

satisfying the failure condition for Ti-6Al-4V would ensure failure of CP Ti as well. The minimum sample diameter was therefore calculated as described below.

$$\sigma = {}^{F}/_{A}\ , A = \frac{\pi d^2}{4}$$

$$\sigma = \frac{4F}{\pi d^2}$$

$$d = \sqrt{\frac{4F}{\pi\sigma}}$$

Where σ is the applied stress in MPa, F is the applied load in Newton, and d is the diameter in mm.

Choosing σ=600MPa, that is above the endurance limit of the Ti-6Al-4V, and considering the maximum capacity of the testing machine that is 3000N, then the diameter is found.

The diameter had to be verified to satisfy the ASTM Standard for fatigue testing.

$$Radius_{curvature} > 8 \times minimumdiameter_{testsection}$$

$$Length_{testsection} > 3 \times minimumdiameter_{testsection}$$

Based on this calculation the sample was designed using the CAD software SolidWorks, 2012 in configuration shown in figure 27.

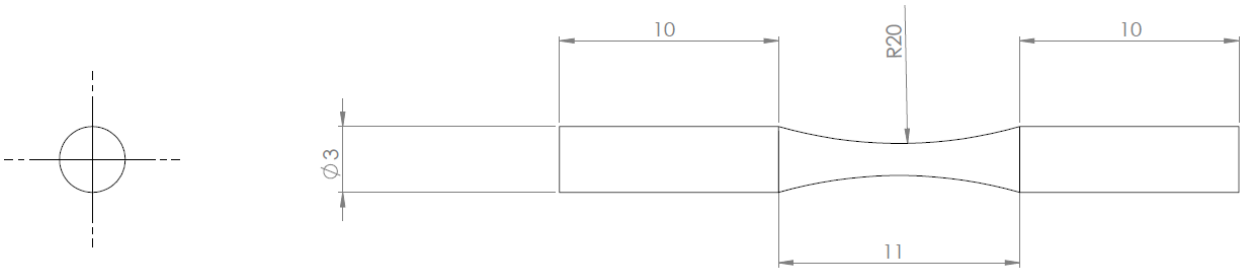

Figure 27. Schematic of the designed specimen prepared by SolidWorks 2012 software.

3.2.2 Machining

A dog-bone shaped sample with the displayed configuration (figure 27) was machined. Since the outer diameter was 3 mm, not all the CNC machine jigs could hold this diameter without undergoing buckling. After many trials, the samples were machined as shown in figure 28.

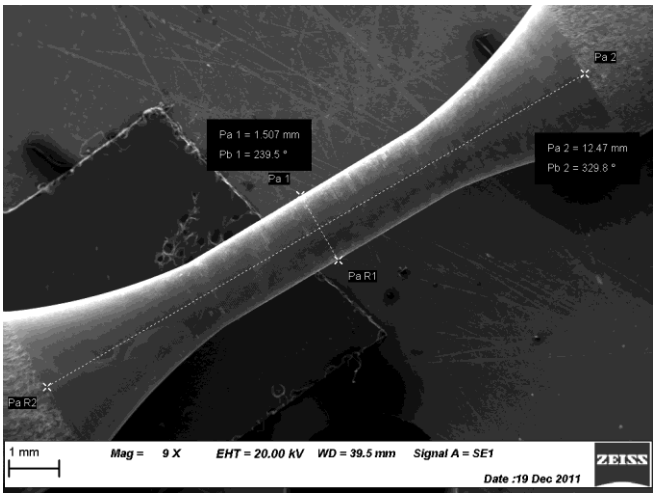

Figure 28. SEM photograph of the machined sample.

3.3 Surface treatments

3.3.1 Mechanical grinding and polishing

By mechanical grinding and polishing, a layer is removed from the surface of the material. Grinding is typically carried out by using silicon carbide abrasive papers with various surface roughness. Coarser papers are used during the first step followed by softer silicon carbide sandpapers. After grinding the material with desired number of steps using various silicon carbide papers, the material is finally polished using a cloth with a solution of diamond paste or Oxide Polishing Suspension (OPS). Achieving better outcome during the last step, the OPS is routinely diluted with an etchant. In order to prevent affecting the surface and titanium oxide layer, electropolishing of the metal was avoided. Due to the dog-bone shape of the material,

polishing on flat plate was impossible. Therefore, a mini lathe was utilized to perform the polishing procedure (figure 29).

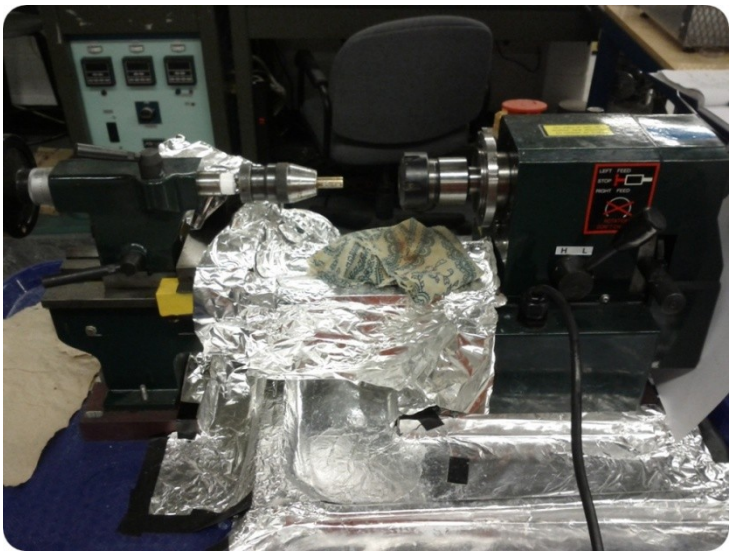

Figure 29. Mini-lathe used for polishing the samples.

CP Ti and Ti-6Al-4V samples were polished in three steps. They were first mechanically grinded using 1200 and 4000 grit silicon carbide sandpapers (Struers, United States). Then, they were polished with a cloth soaked in a mixture of 0.05 micron colloidal silica suspension (Anamet, Montreal, Quebec, Canada) and Hydrogen Peroxide, H_2O_2 (Fisher Scientific, MA, USA).

3.3.2 Anodization

By capitalizing on previous work with anodization, the following parameters were chosen for treating CP Ti and Ti-6Al-4V. Each specimen was anodized in 0.5% hydrofluoric acid (HF) solution at 20 Volts for 30 minutes. In this process titanium was connected to the anode port of the DC Power Supply (1697 Programmable Switching DC Power Supply 1-40V, B&K Precision, CA, USA) and a steel beaker was used as cathode that can be seen in figure 30.

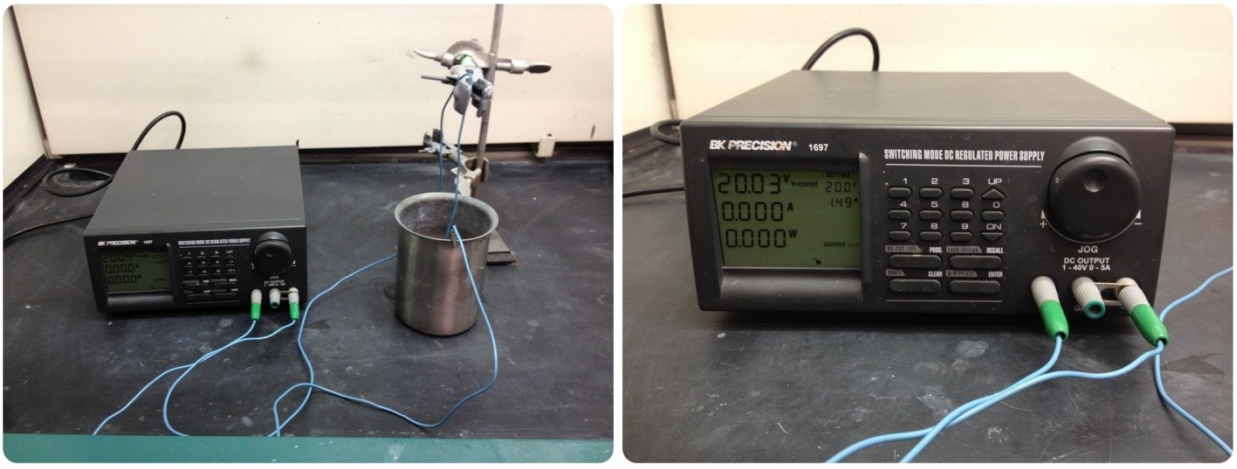

Figure 30. Anodization process, including in the image are power supply, sample (anode), steel beaker (cathode), and the power supply.

The result of this process is the formation of an oxide layer in the form of nanotubes on the surface of CP Ti and Ti-6Al-4V.

3.3.3 Oxidative nanopatterning

As stated in section 2.6.3, many studies have been carried out in order to develop nanofeatures on the surface of the biomedical implants. Oxidative nanopatterning is one of the methods by which a sponge-like structure composed by nanosized pores is created on the surface of Ti-based metals. In this process, Piranha solution, mixture of sulfuric acid (H_2SO_4) and hydrogen peroxide (H_2O_2) in different ratios, is utilized to etch the surface of the material and create nanopits. Polished CP Ti and Ti-6Al-4V were nanopatterned by immersing the samples in the etching solution with ratio of 1:1 of H_2SO_4 (Sulfuric acid, 96%, VLSI grade, Honeywell, Phoenix, USA) and H_2O_2 (Fisher Scientific, MA, USA) for 2 hours and 30 minutes under moderate stirring. Piranha solution's temperature rises immediately after mixing both chemicals, therefore to avoid boiling of the solution during the treatment it was ice-cooled prior to sample immersion to a

temperature of 12°C. As the treatment progresses the white color of the piranha solution turns yellow and its temperature rises above room temperature. The process of oxidative nanopatterning can be seen in figure 31.

Figure 31. Beakers containing piranha solution and titanium samples on stirring plate at the end of oxidative nanopatterning process for 2.5 hours.

3.3.4 Other results with oxidative nanopatterning and anodization

To assess calcium adsorption possibilities on the surface of CP Ti and Ti-6Al-4V the calcium-based solution was provided and used for both processes of anodization and oxidative nanopatterning. Table 9 represents the composition of each solution and the relevant utilized surface modification technique.

Table 9. Calcium-based solutions' compositions and the relevant applied surface treatment.

Nanopatterning technique	Chemical solution
Oxidative nanopatterning	0..96%H_2SO_4+CaO_2(calcium peroxide)
Anodization	0.85%H_3PO_4+0.5%HF+$CaCO_3$(calcium carbonate)
Anodization	0..96%H_2SO_4+0.5%HF+ CaO_2(calcium peroxide)
Anodization	0.5%HF + each of the following products in separate solution • CaO_2(calcium peroxide) • $CaCO_3$(calcium carbonate) • $Ca(OH)_2$(calcium hydroxide) • $Ca_3(PO4)_2$(calcium phosphate)

3.4 Fatigue testing procedure and equipment

Laboratory fatigue tests can be performed in different ways which have been detailed in section 2.3. For evaluating the fatigue life of the treated and polished CP Ti and Ti-6Al-4V samples, computer controlled fatigue testing machine has been used.

The equipment used to carry out the fatigue tests was from the new series of Instron ElectroPuls™ Fatigue Testing Instruments (Instron, MA, USA). The type of the instrument is Instron All-Electric ElectroPuls™ E3000 with the maximum dynamic capacity of ±3KN and maximum frequency of 100Hz which is made exclusively for performing fatigue testing. The Wavematrix Software specifically made for fatigue testing by Instron was utilized for the testing process.

In order to calculate the load to be used during the test, the diameter of each sample was measured using the optical microscope. Several diameter sections in the narrowest part of the sample were measured to accurately assess the diameter of the narrowest section.

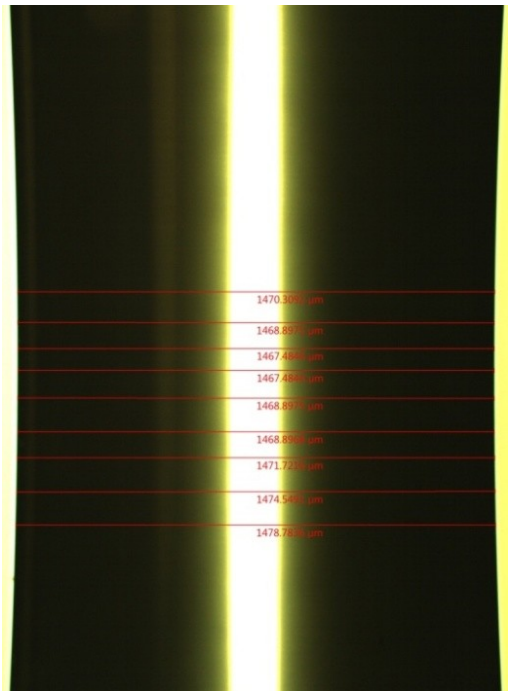

Figure 32. Process of measuring the diameter of the narrow section of dog-bone shaped samples using the optical microscope.

Stress levels have been chosen to be above the endurance limit of the material, and based on the cross sectional area of each specimen the required constant load amplitude was calculated. The frequency for axial fatigue testing of CP Ti was 10Hz, but since the stress level for Ti-6Al-4V was about twice that of CP Ti this frequency was too high for that stress level and the machine could not perform the full cycle. To overcome this limitation, the selected frequency for Ti-6Al-4V was chosen as 5Hz to be able to perform the full cycle.

The grips of the fatigue machine were meant to test flat samples and were not suitable to test the cylindrical sample used in this Thesis. Two sets of sample holders were therefore designed to increase the contact surface area between the sample and the grips and to prevent the sample from sliding in the grips. These sample holders were made of stainless steel and were sandblasted to increase the friction and thus further prevent the sample from sliding. The fatigue testing set up of the machine can be seen in figure 33.

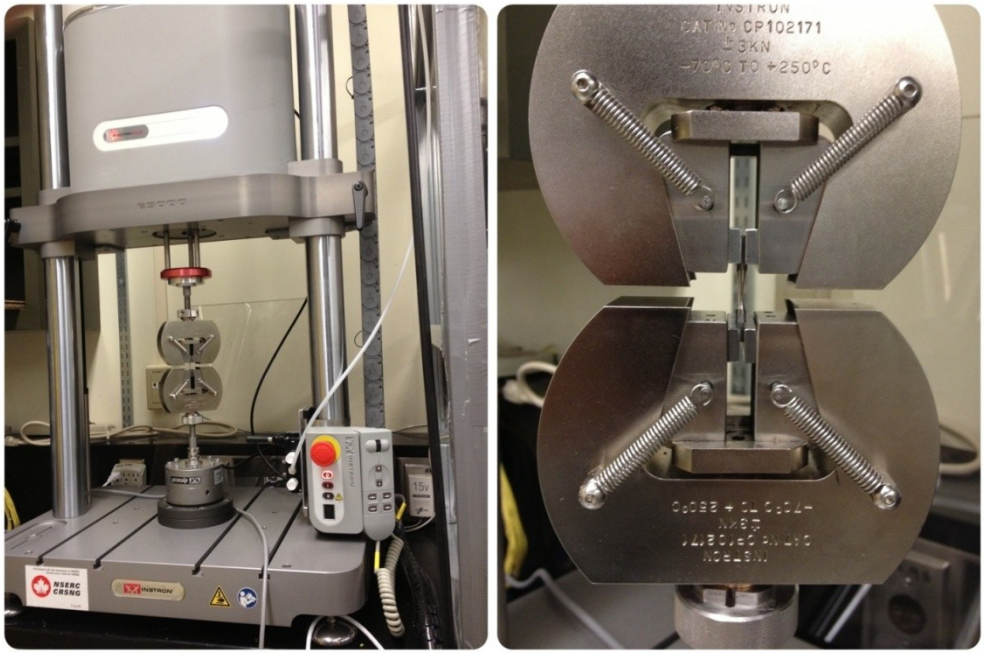

Figure 33. All-Electric ElectroPuls™ E3000 Instron fatigue testing machine and a sample located between the grips for testing.

3.5 SEM analyses

To better study the nanotopographies created by the anodization and oxidative nanopatterning, as well as the fractured surface of the material failed due to fatigue failure, a Scanning Electron Microscope (JEOL, JSM-7500F) was utilized. Samples prepared for imaging were categorized into six groups. Each sample from each of these six groups shown in table 6 was analyzed on both of the side of the samples and its cross section after failure. Side imaging is required to study the effects of fatigue process on each treatment, while the cross sectional imaging revealed that fatigue failure characteristics. This made a total of twelve cases of SEM imaging groups and subgroups. Further sample cleaning was avoided to prevent any modifications of the surface topographies. Best quality of the desired images was obtained by setting the SEI mode with working distance (WD) of 3 mm and voltage of 3KV.

The images obtained using a JSM-7500F scanning electron microscope located at Centre for Catalysis Research and Innovation (CCRI) laboratory at the University of Ottawa.

Chapter 4 Experimental Results

4.1 Surface treatments

4.1.1 Polishing

4.1.1.1 Microstructure of the polished samples

After polishing the samples and following the procedure explained in section 3.1.2, the microstructure of the CP Ti grade 2 and Ti-6Al-4V was characterized by optical microscopy. Images revealed an equiaxed structure for both metals (figure 34). As Akahori *et al.* found (section 2.4.1) the equiaxed microstructure exhibits a superior fatigue performance than lamellar. The equiaxed microstructure is obtained by annealing CP Ti and Ti-6Al-4V as-received samples to temperature above 882°C. The higher endurance limit of the equiaxed microstructure than lamellar is because of the smaller size of the grains and higher numbers of them. The average grain size of CP Ti and Ti-6Al-4V were estimated by utilizing Heyn Lineal Intercept Procedure provided by the American Society for Testing and Materials (ASTM) International standards designation E112-12 Standard, i.e. *Standard Test Methods for Determining Average Grain Size.* The average size of the grains for CP Ti and Ti-6Al-4V are therefore found to be 24 μm and 4 μm respectively.

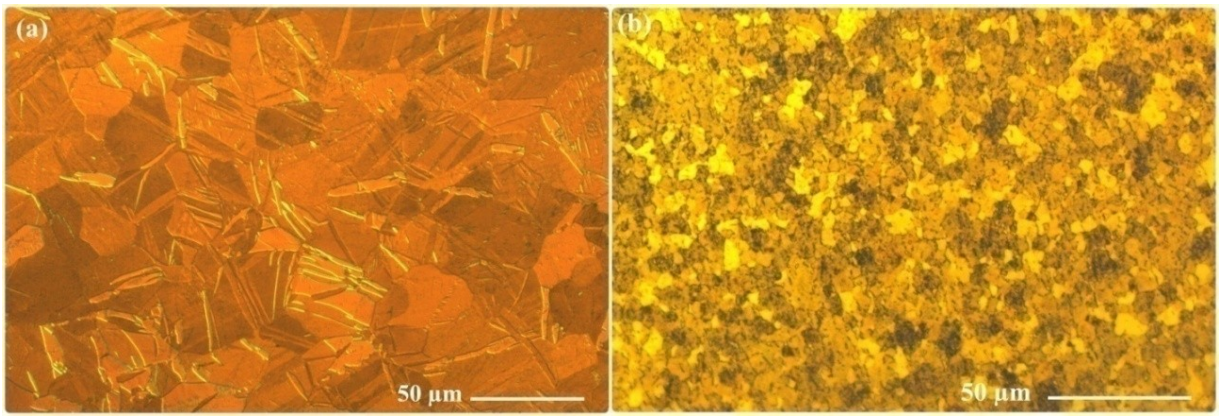

Figure 34. Equiaxed microstructure of (a) commercially pure titanium grade II (CP Ti), and (b) Ti-6Al-4V alloy.

4.1.1.2 Surface finish of the polished samples

Results obtained from the fatigue testing of the machined samples were so scattered, which was due to the fact that fatigue behavior is very sensitive to surface inhomogenities and machined samples were assumed to carry some surface defects created during machining process. To eliminate the surface machining marks and other possible surface defects, both materials were polished step by step through the procedure explained in 3.3.1. Mechanical polishing of the samples removed any undesired surface features such as machining marks. Samples were mechanically polished to rule out the effects of surface roughness from the evaluation of the fatigue behavior. Figure 35 displays the surface finish of the machined and polished samples. Polished samples were then used as reference for the assessment of the fatigue resistance of chemically treated samples.

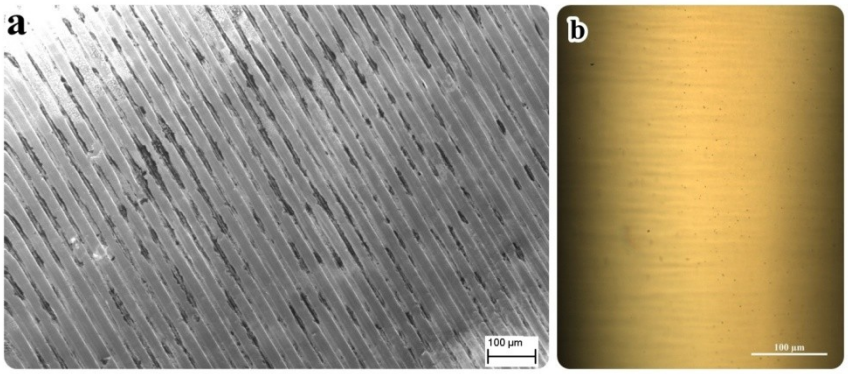

Figure 35. Removing machining marks from the surface of the material by mechanical polishing. a) Surface of the material prior to polishing, b) Surface of the material after polishing.

4.1.2 Anodization in 0.5% Hydrofluoric acid (HF)

4.1.2.1 Morphological analysis of CP Ti and Ti6-Al-4V (SEM)

Mechanically polished CP Ti and Ti-6Al-4V were anodized according to the protocol outlined in section 3.3.2. Anodized surfaces exhibited uniformly distributed arrays of titania nanotubes (figure 36). The average diameter of the nanotubes and their approximate length were measured by using image analysis software (ImageJ). A circularity coefficient (i.e. two-dimensional geometric parameter that defines how much an object can deviate from a full circle, to which a circularity of 1.0 is assigned) greater than 0.5 (to avoid including any undesired shapes, such as β-phase grains in case of Ti-6Al-4V, in diameter estimation) and an area greater than 0.004μm^2 (to avoid including any small objects mistakenly recognized by the software as nanotube diameter) were chosen for the analysis. Results from these measurements determined that the average CP Ti nanotube diameter is 86±9 nm.

The same procedure was adopted for the Ti-6Al-4V alloy. The average diameter was found to be 78±6 nm.

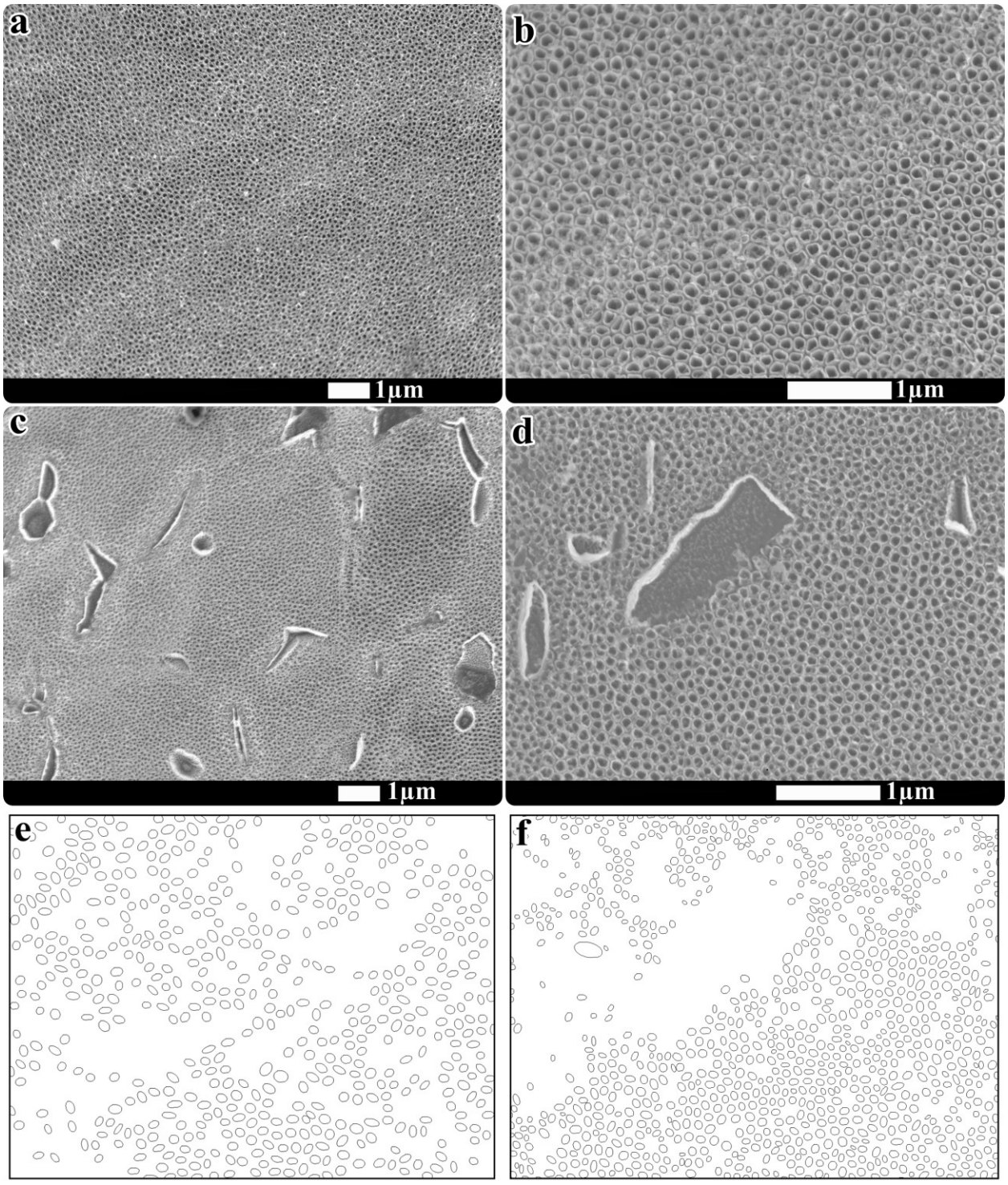

Figure 36. Uniformly distributed arrays of nanotubes created by anodization on the surface of CP Ti (a-b) and Ti-6Al-4V (c-d). Preferential removed β-phase grains can be observed on the surface of the alloy (c-d). Images (e) and (f) are masks of images (b) and (d) with the same scale and display the nanotubes which complied with the chosen parameters for image analysis (i.e. circularity > 0.5 and area > 0.004µm2), for CP Ti and Ti-6Al-4V, respectively.

The average length was estimated to be 210±13 nm for Ti-6Al-4V and 380±16 nm for CP Ti. This value was obtained by measuring the length of exfoliated nanotubes that laid parallel to the surface, thereby enabling the estimation of their length by SEM imaging.

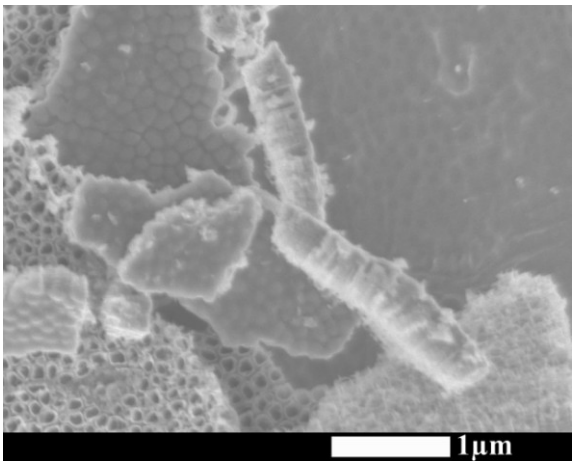

Figure 37. SEM micrograph demonstrating detached nanotubes that laid parallel to the surface, used to estimate their length.

The size distribution of the nanotube diameter was finally plotted in a histogram (figure 38).

In the case Ti-6Al-4V, SEM analysis also revealed the presence of microcavities, likely associated to a preferential and more aggressive attack of β-phase grains.

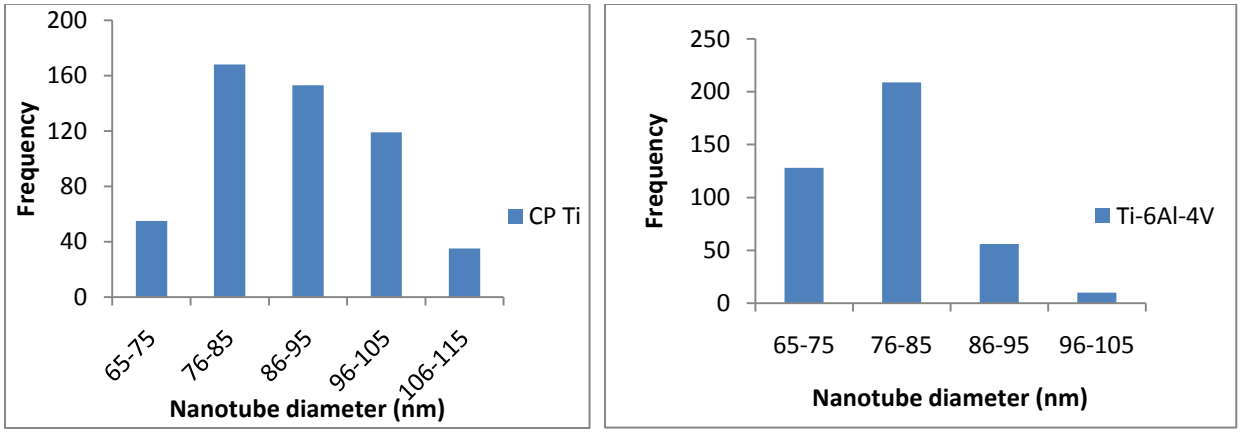

Figure 38. Size distribution of the nanotube diameter for CP Ti and Ti-6Al-4V.

4.1.3 Oxidative nanopatterning with Piranha (H_2SO_4/H_2O_2) solution

4.1.3.1 Morphological analysis of CP Ti and Ti6-Al-4V (SEM)

Exposing CP Ti and Ti-6Al-4V to the Piranha solution for 2.5 hours yielded a sponge-like surface composed by a homogenous network of nanosized pits (Figure 39)

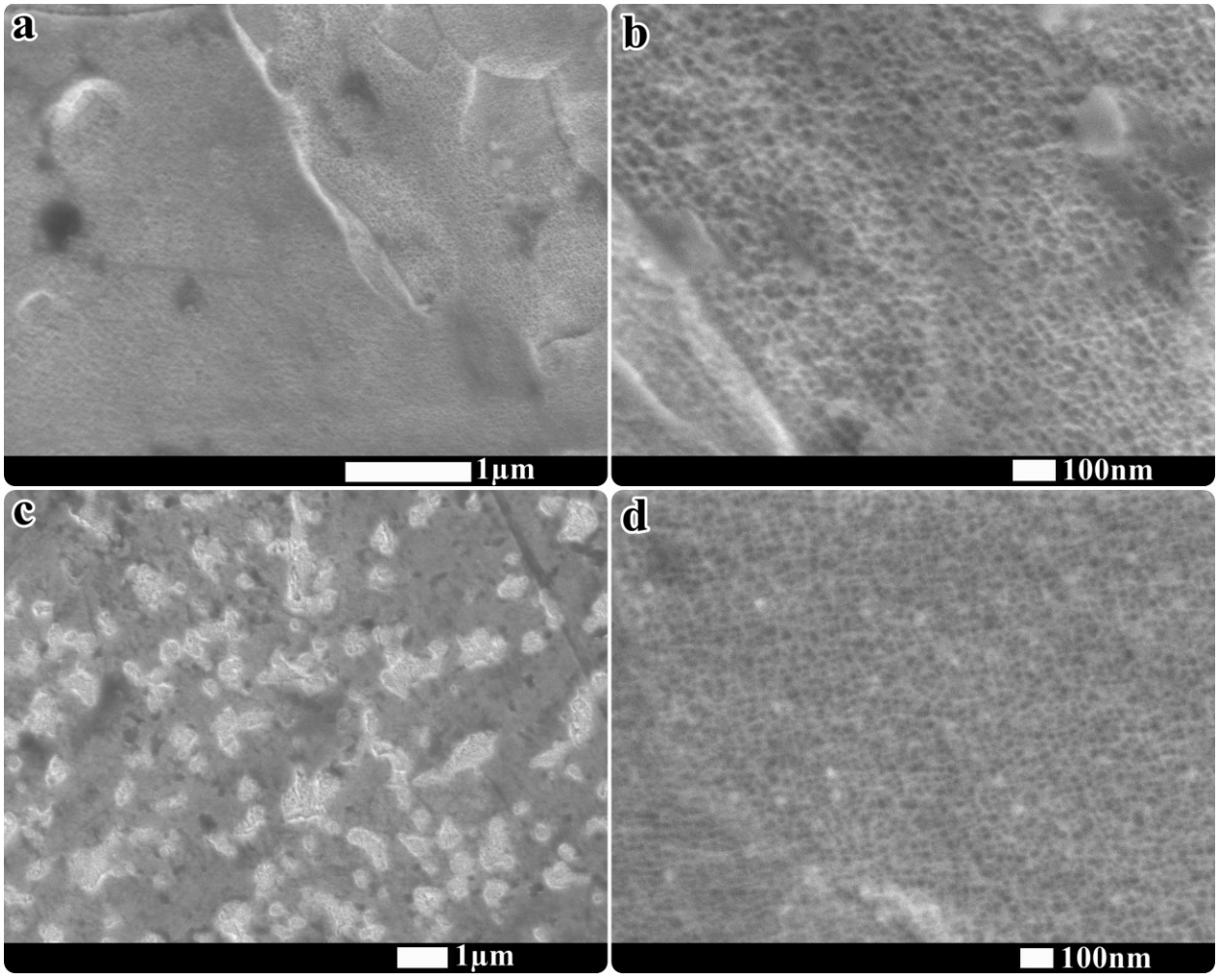

Figure 39. Sponge-like surface created by oxidative nanopatterning on the surface of CP Ti (a-b) and Ti-6Al-4V (c-d).

As stated in section 2.6.3, Variola *et al.* characterized the nanotextured features on both metals and found that the diameter of nanopits after 2 hour exposure for CP Ti and Ti-6Al-4V were respectively 20-22 nm and 21±7 nm [43][44]. Although the two metals did not differ in terms of nanopits diameter, the presence of micrometric cavities on the surface of the alloy, resulting from a selective attack of the β-phase grains, generated a micro-topography (figure 39 c), which was not found on CP Ti. This confirmed that etching rate of β-phase during oxidative nanopatterning is higher than α-phase [44]. Visual comparison of SEM images of treated alloy samples suggests that anodization yields deeper β-phase grain cavities when compared to those generated by oxidative nanopatterning (Figure 40).

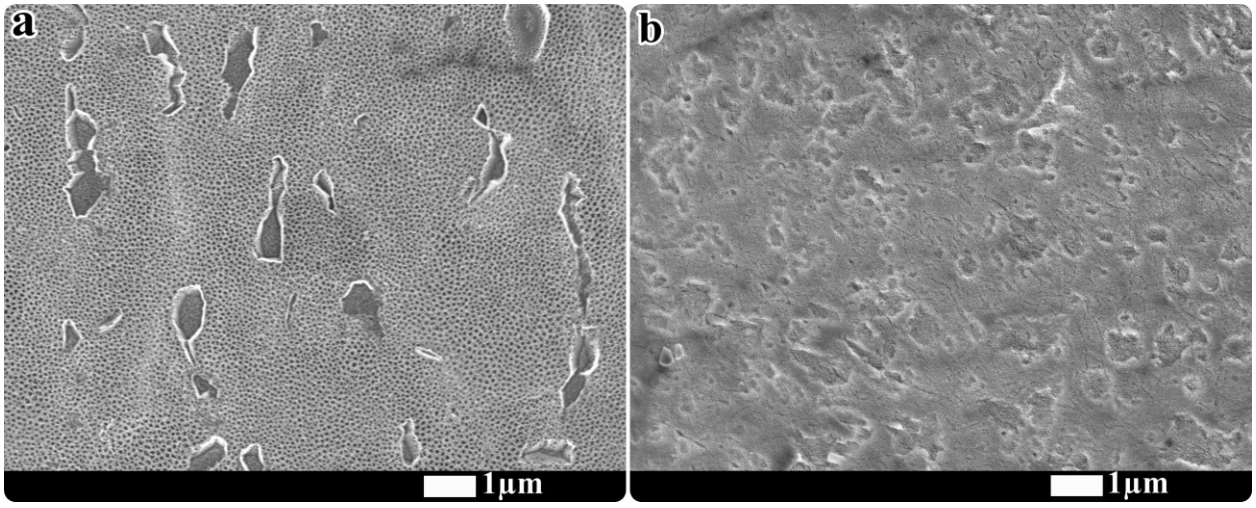

Figure 40. Microcavities on the surface of the Ti-6Al-4V generated by (a) anodized and (b) oxidative nanopatterning.

4.1.4 Fatigue behavior of CP Ti and Ti-6Al-4V

4.1.4.1 S-N curves

The cyclic stress plotted against the logarithmic scale of cycles to failure, i.e. S-N curves (see section 2.3.1), was obtained for both pristine and chemically modified metals. These curves help the reader to not only study the fatigue behavior of each material independently, but also to compare surface treatments effects on the fatigue life of the material. To assess the effects of polishing on the overall fatigue resistance, the S-N curves for reference polished samples were compared to those found in literature (figure 41). Our results indicate a consistency between the control samples utilized in our tests and those previously published [8]. As one may notice in obtained S-N curves, that are very similar to previous studies on fatigue behavior of the materials available in the literature, there is only one data point in each stress level. The reason is since fatigue tests are time consuming, it would have been taken several months for each test to be accomplished if we were to have few data points in each stress level.

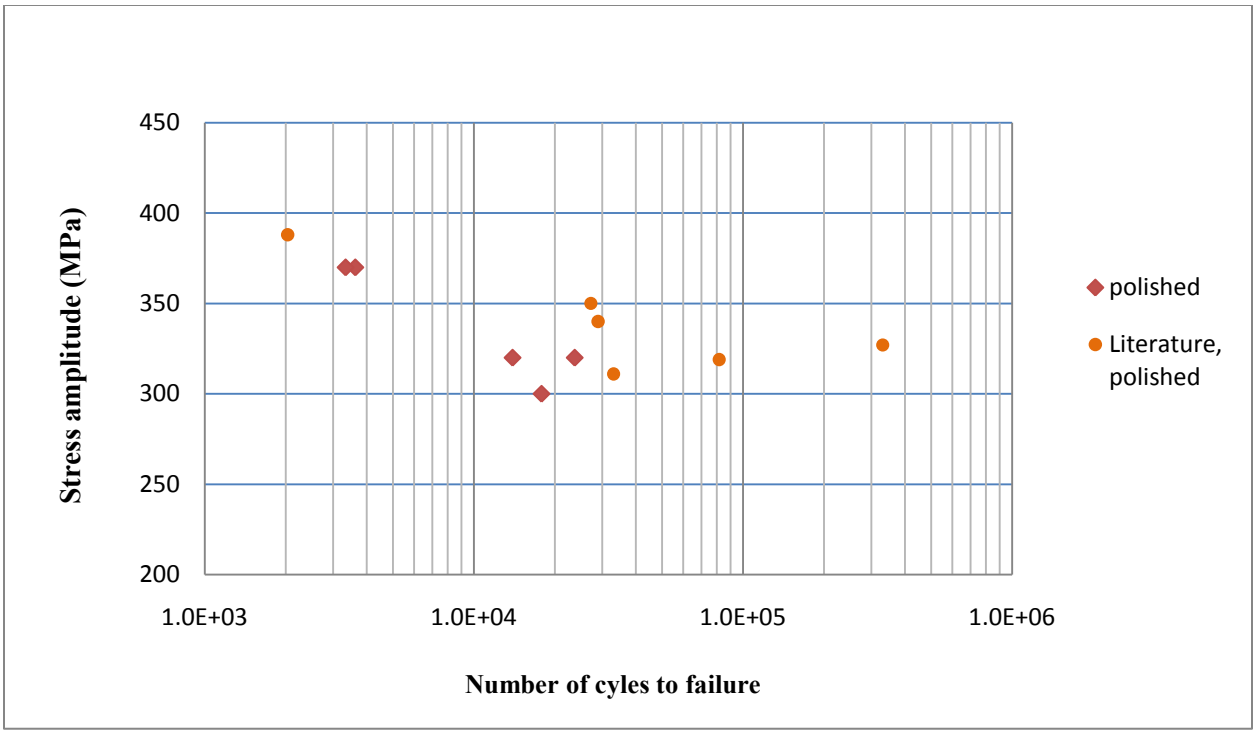

Figure 41. Assessing the consistency of fatigue behavior of the reference polished samples with previous work [8].

In the case of chemically treated samples, while the resulting surface features did not significantly affect the fatigue resistance of CP Ti (figure 42), that of the Ti-6Al-4V alloy was influenced by the technique employed (figure 43). In particular, the S-N curves suggest that, compared to polished samples, both anodization and oxidative nanopatterning impact negatively the fatigue resistance of the alloy, with more deleterious effects associated to the former technique.

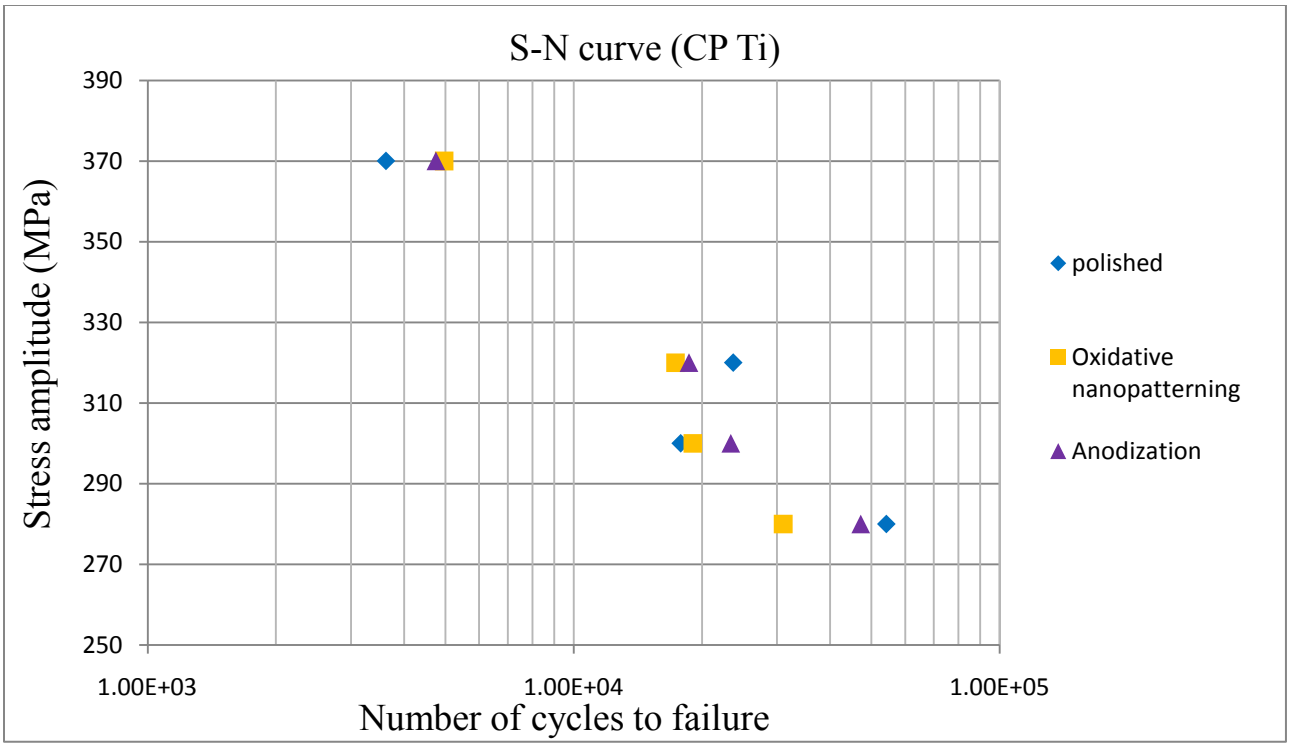

Figure 42. S-N curves of control and chemically modified CP Ti

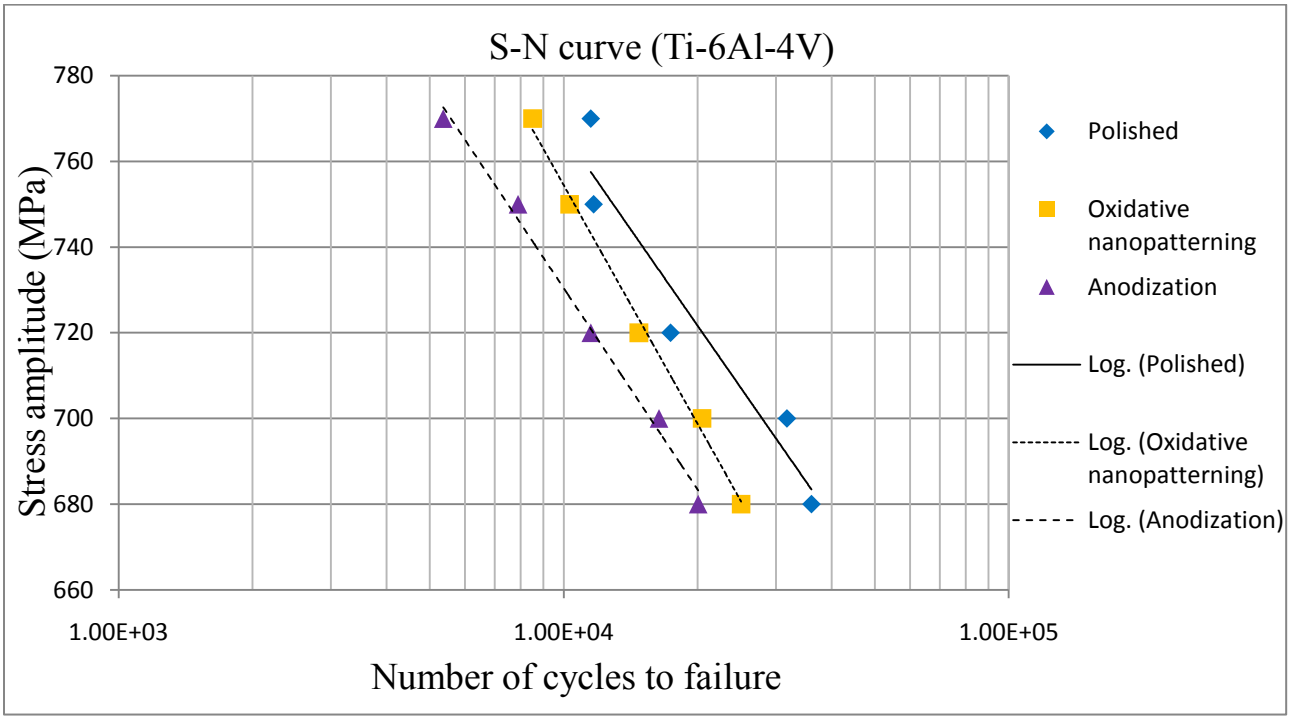

Figure 43. S-N curves of control and chemically modified Ti-6Al-4V.

4.1.4.2 Morphological and fracture surface analysis (SEM)

Although S-N curves provide valuable information about the fatigue behavior of the metal, further analysis is required to investigate the morphological changes due to fatigue cyclic loading. To this end, SEM investigation provides important evidence of the response of both the bulk material and oxide layer to fatigue failure. In addition, images from fractured surfaces generate information about crack nucleation, propagation, and fatigue failure characteristics.

Images taken from the fracture surface of both metals show crack initiation sites and their propagation path until fatigue failure. Beachmarks and striations are clearly visible in SEM micrographs (figures 44-45 b, d and f), an evidence of fatigue failure of the material.

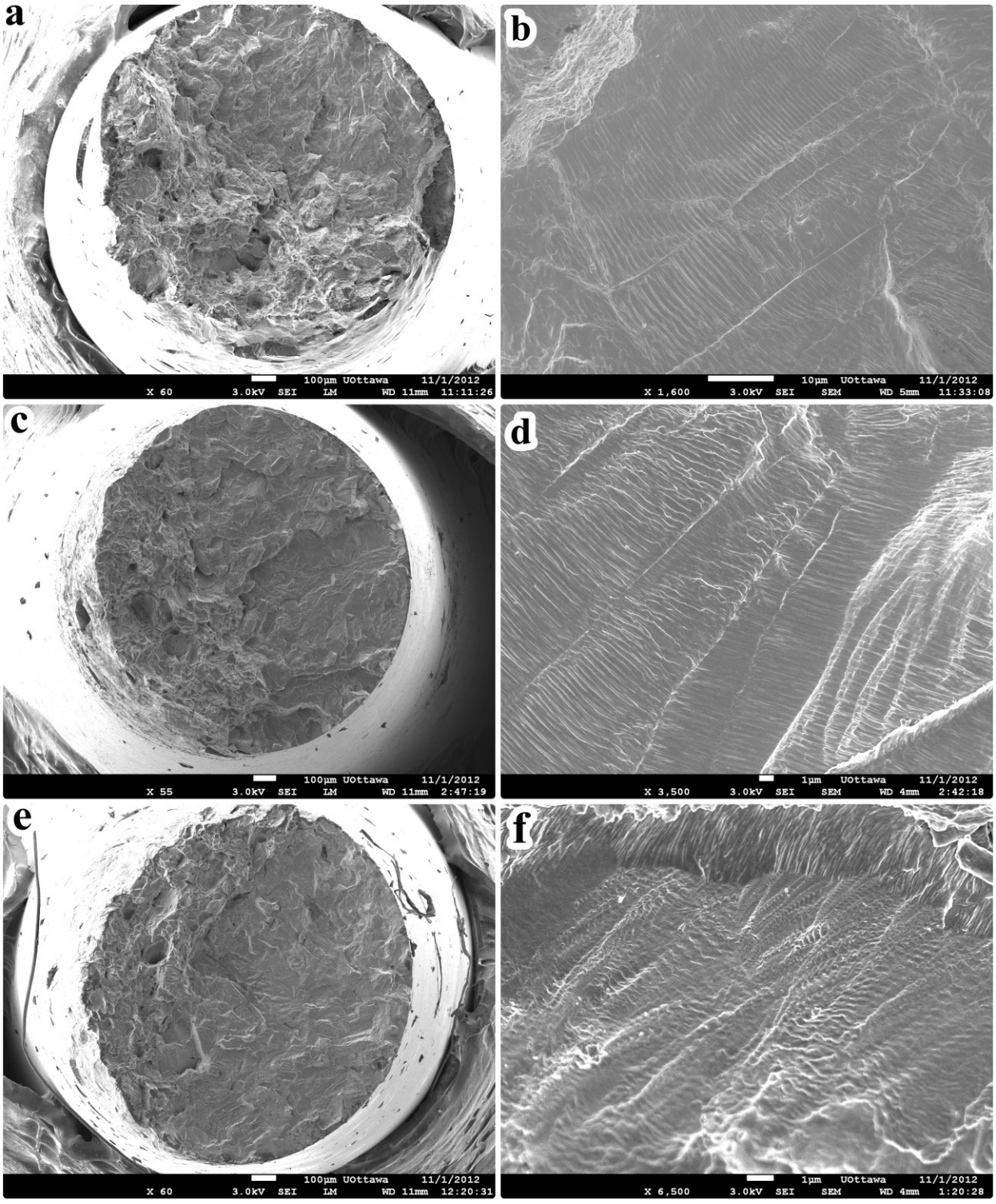

Figure 44. SEM images of the fracture surface of (a, b) polished, (c, d) anodizaed and (e, f) nanopatterned CP Ti. Images of the right column were taken at a higher magnification. Beachmarks and striations are visible (b, d and f). Cracks propagated inwards across the cross section of the samples, until fracture occurred.

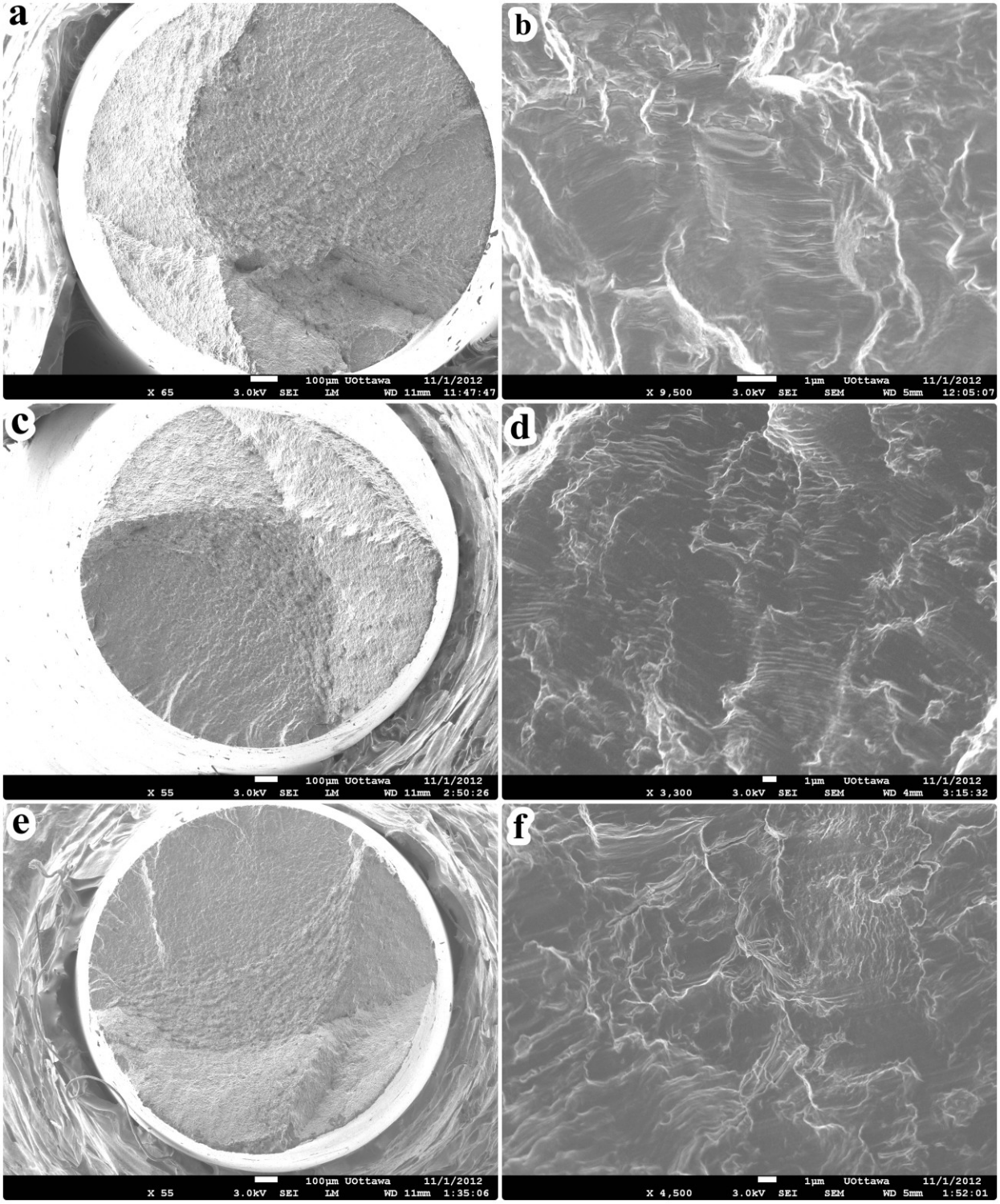

Figure 45.SEM images of the fracture surface of (a, b) polished, (c, d) anodizaed and (e, f) nanopatterned Ti-6Al-4V. Images of the right column were taken at a higher magnification. Beachmarks and striations are visible (b, d and f). Cracks propagated inwards across the cross section of the samples, until fracture occurred.

The effects of cyclic load on the material surface, and in particular on the integrity of the superficial oxide layer, are presented in figures 46-47, for CP Ti and Ti-6Al-4V, respectively. These images have been ordered to display the evolution of damage, from the farthest point to the closest point to the fracture surface. As the distance to the fracture surface decreases, cracks on the oxide layer increase in number and dimension. These started as isolated cracks, which eventually joined together to generate bigger crevices. This ultimately yielded significant exfoliation of the oxide layer, with islands of adherent and intact nanotubes surrounded by the bare metallic surface.

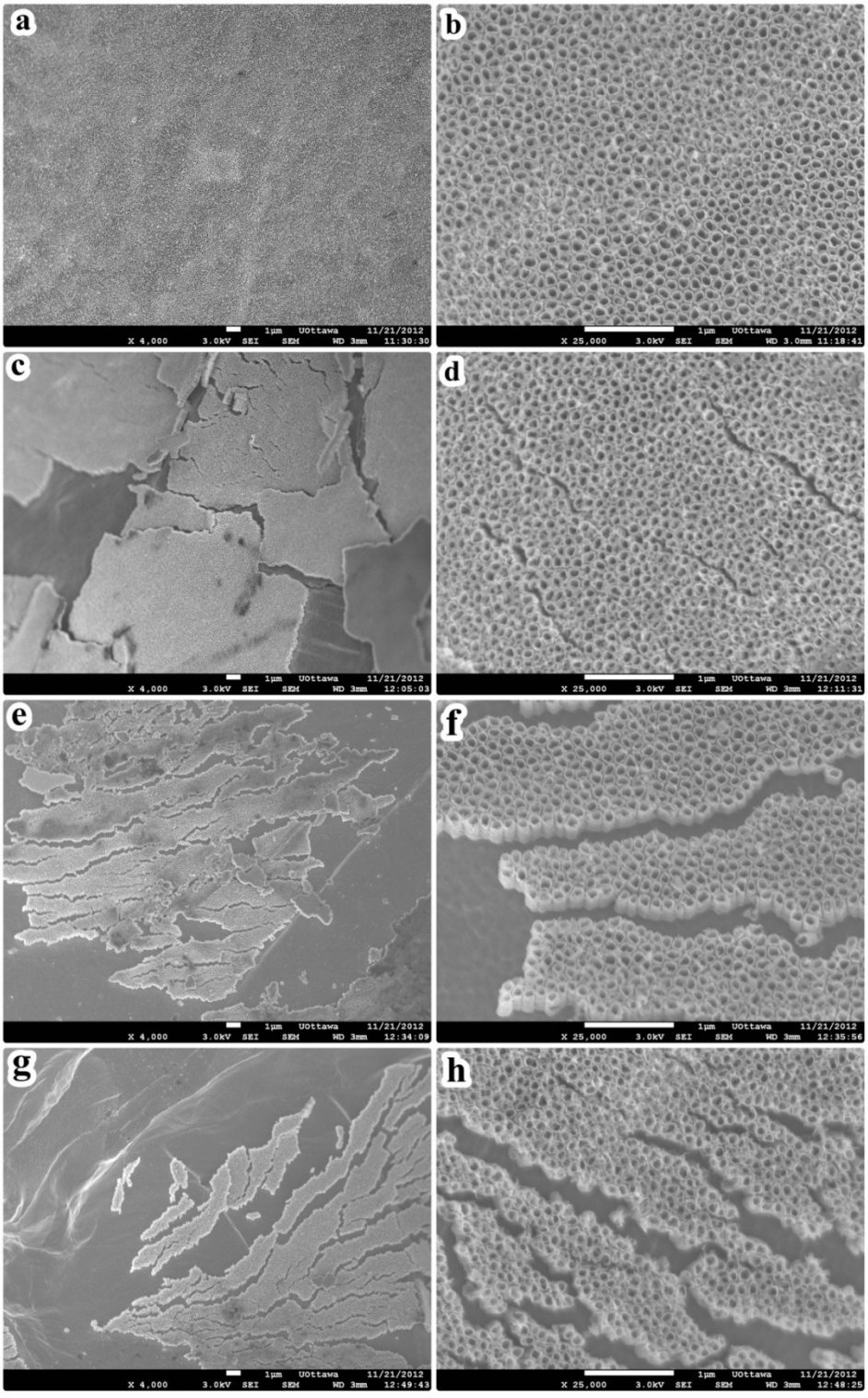

Figure 46. SEM micrographs illustrate the effects of cyclic loads on the CP Ti oxide layer as increasingly moving from the farthest point (a-b) to the closest point (g-h) to the fracture surface. Images of the right column were taken at a higher magnification. Small cracks initiated and developed along the walls of nanotubes at sites distant from the fracture (c-d) and increased in number and size closer to the fracture surface (f-g), until significant exfoliation occurred (e-h).

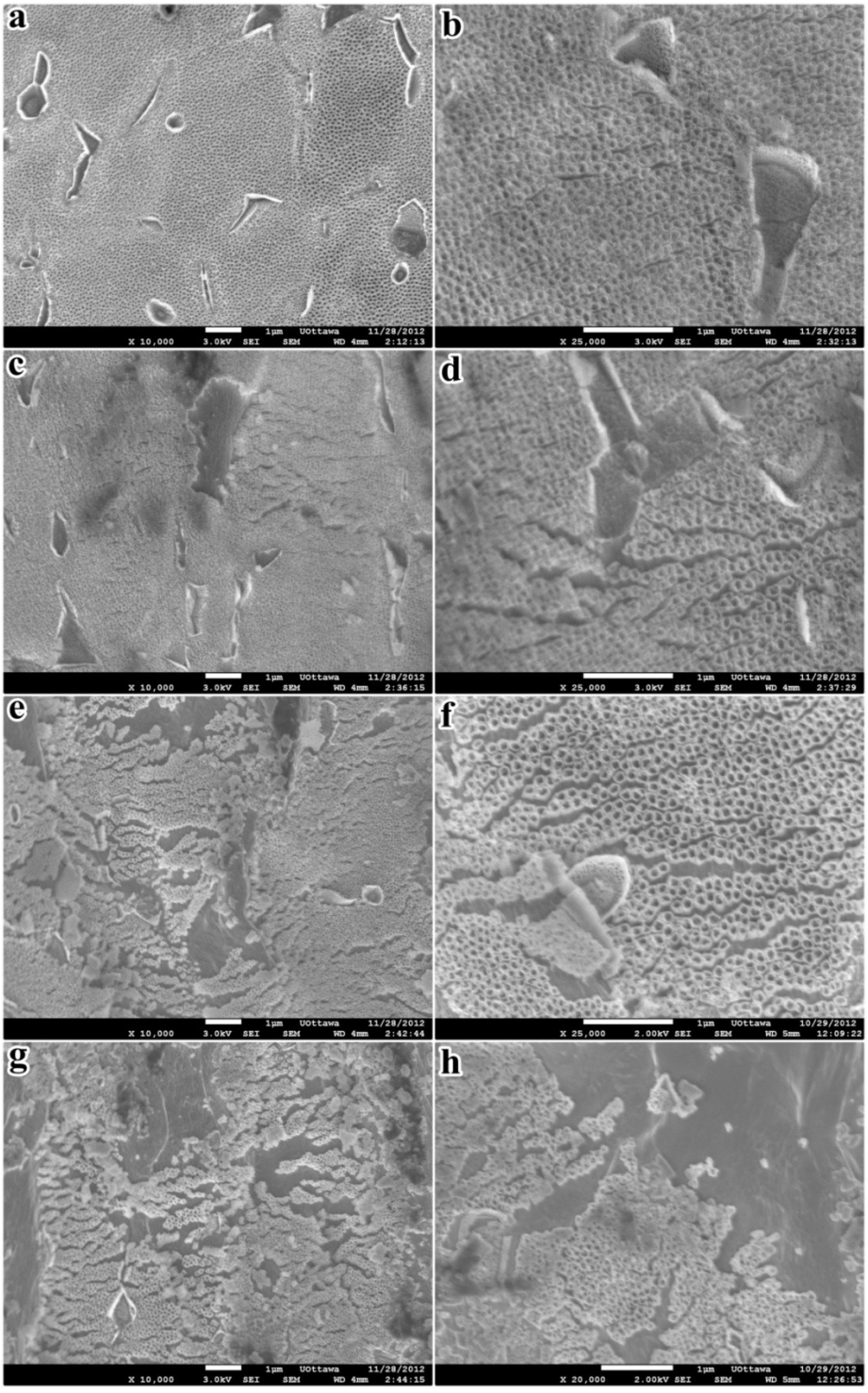

Figure 47. SEM micrographs illustrate the effects of cyclic loads on the Ti-6Al-4V oxide layer as increasingly moving from the farthest point (a-b) to the closest point (g-h) to the fracture surface. Images of the right column were taken at a higher magnification. Small cracks initiated and developed along the walls of nanotubes at sites distant from the fracture (c-d) and increased in number and size closer to the fracture surface (f-g), until significant exfoliation occurred (e-h). Oxide layer damaging was not influenced by the dual phasic nature of the alloy (in α and β phase grains).

Scanning electron microscopy analysis of samples subjected to oxidative nanopatterning highlighted the presence of microcracks which initiated and propagated on metal surface (figures 48-49). The effects on cyclic loads impacted the integrity of the oxide layer to a lesser extent as compared to anodized samples.

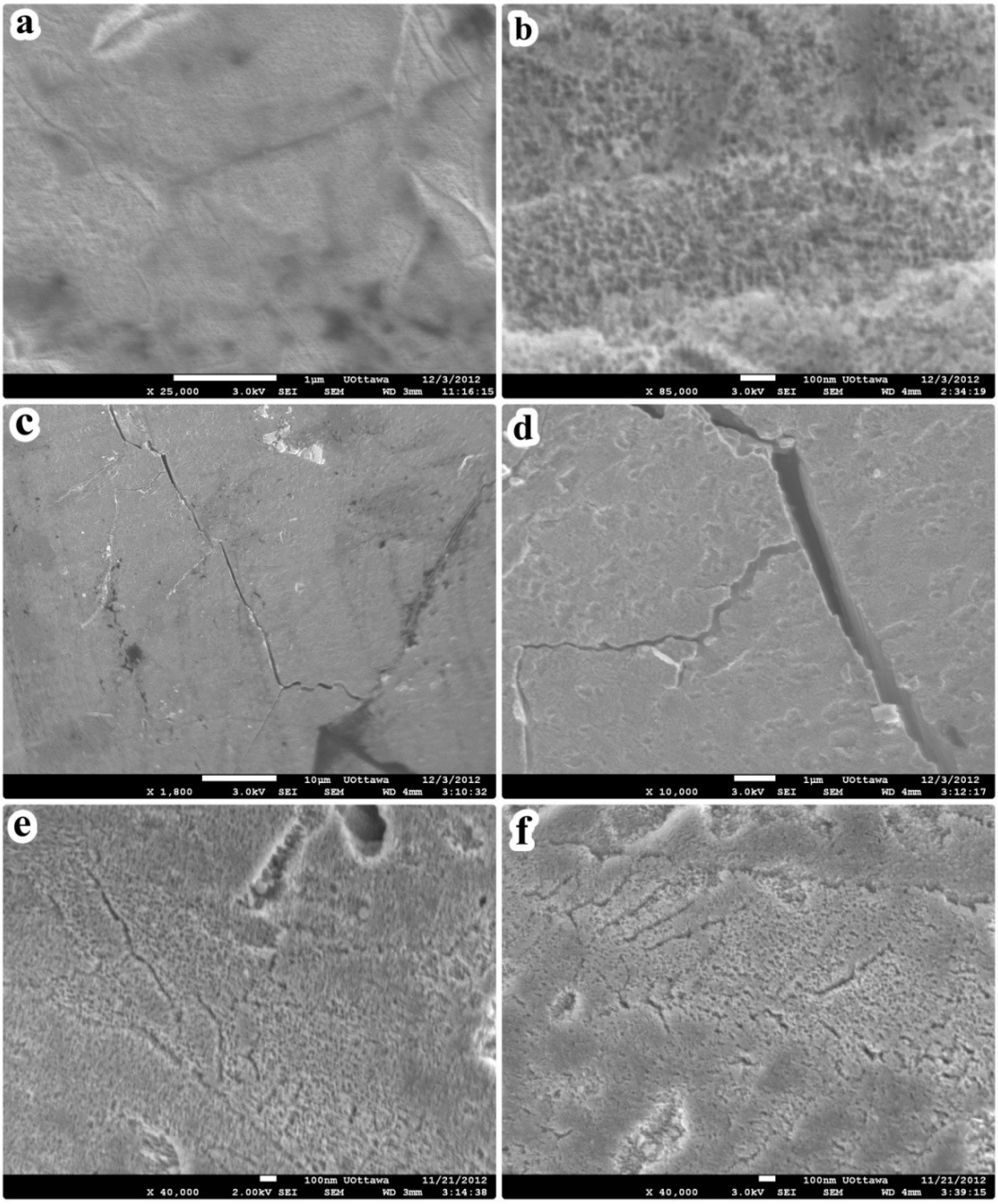

Figure 48. SEM images of CP Ti samples subjected to oxidative nanopatterning. Images are ordered from the farthest (a) to the closest (f) site in relation to the fracture surface. Fracture in the bulk metals is visible in (c-d).

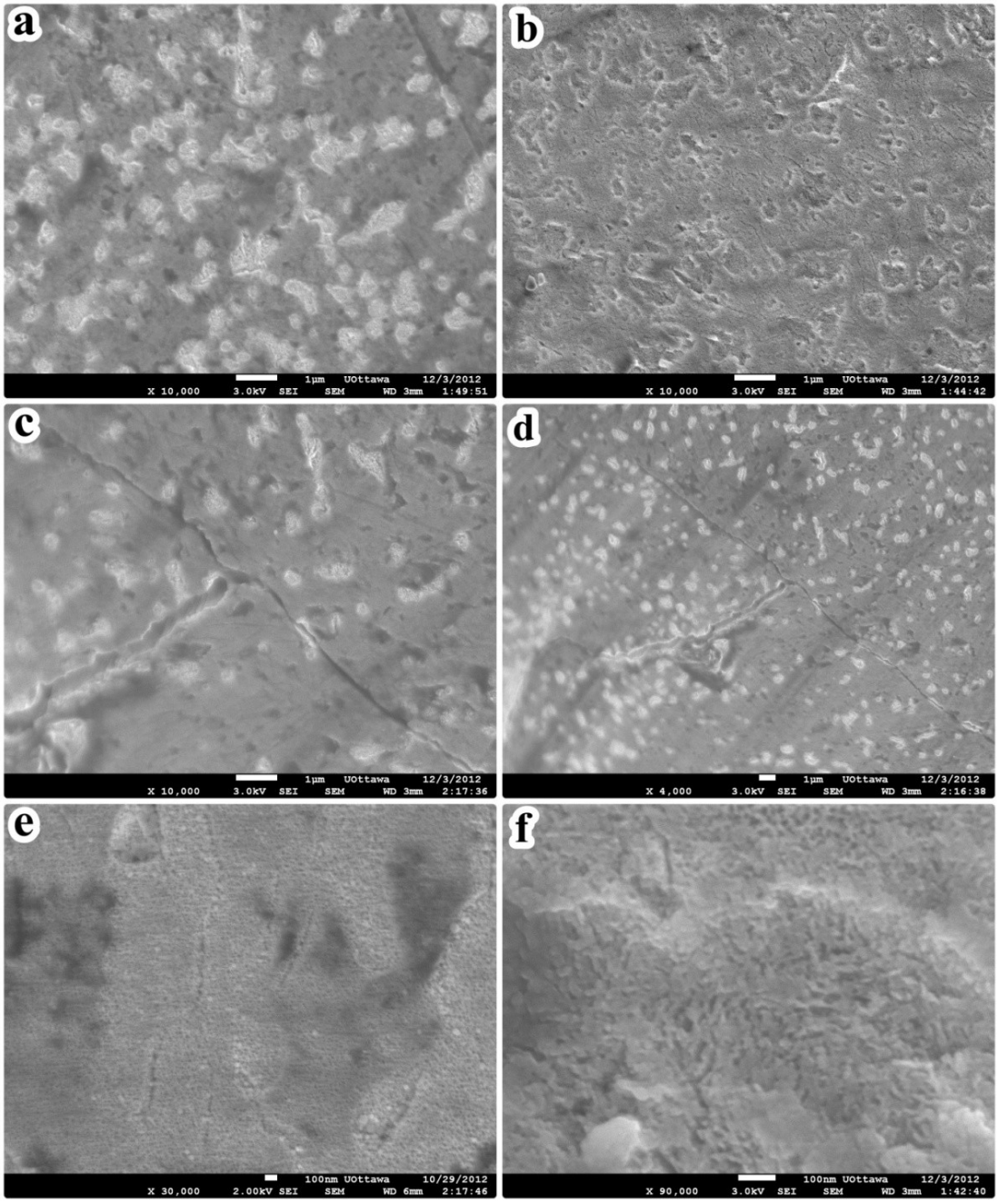

Figure 49. SEM images of Ti-6Al-4V samples subjected to oxidative nanopatterning. Images are ordered from the farthest (a) to the closest (f) site in relation to the fracture surface. Fracture in the bulk metals is visible in (c-d).

4.1.4.3 Stress flow throughout the surface of CP Ti and Ti-6Al-4V

Stress analysis was required to investigate quantitatively the effects of stress variation on the oxide layer along the sample. This analysis revealed the stresses at which the cracks were first observed on the oxide layer (figure 50). In the case of CP Ti, the first cracks were seen at 237±28 MPa on anodized samples and at 241±29 for the nanopatterned ones. These values significantly varied in the case of the Ti-6Al-4V alloy, increasing to 658±28 MPa and 638±50 MPa for anodized and nanopatterned samples, respectively. These values were obtained by SEM analyses followed by stress calculation. In other words, utilizing SEM and moving from the end of the sample to the fracture point, first cracks were found on the oxide layer created on the surface of the metal by anodization. Then, the diameter and consequently the cross sectional area, corresponding to the point where the crack was seen, was calculated. Finally, having the cross sectional area and knowing the load applied to the metal, the relevant stress was obtained. Instead of turning samples to search for cracks at each level, different samples were used to find the stress at which first cracks were observed.

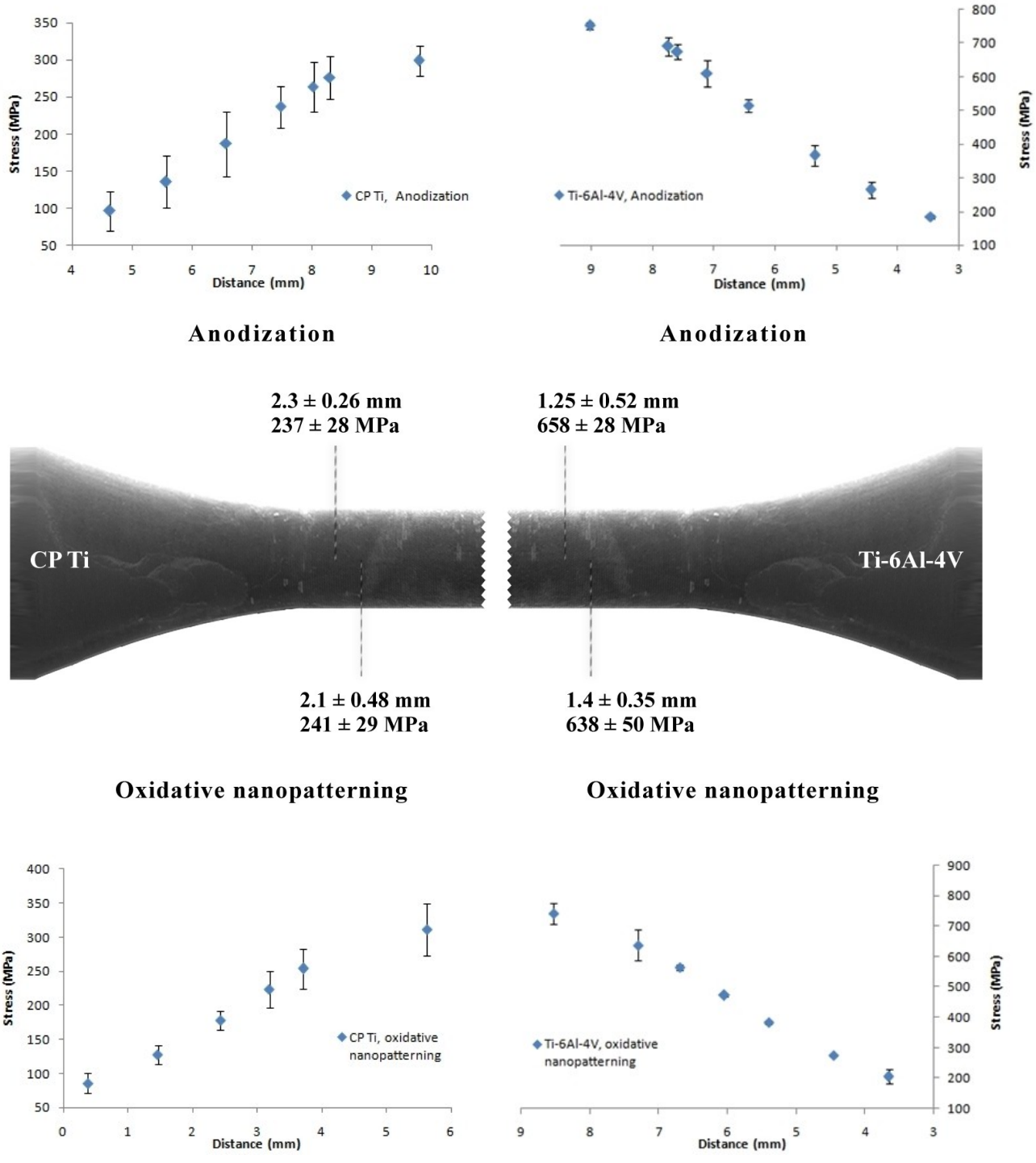

Figure 50. Stress profile versus distance and the stress (and corresponding distance from fracture) at which the first cracks are observed can be seen. Numbers around the schematic of the dog-boned shaped sample indicates the distance and the stress at which the first cracks were seen.

4.1.4.4 Anodized oxide layer behavior in response to fatigue failure process

The effects of fatigue failure on CP Ti and Ti-6Al-4V oxide layers were also assessed by evaluating the area fraction of the pristine nanotubes to the surface of the material. This evaluation was repeated in six different positions along the sample, and correlated to the local stress level (figure 51-52).

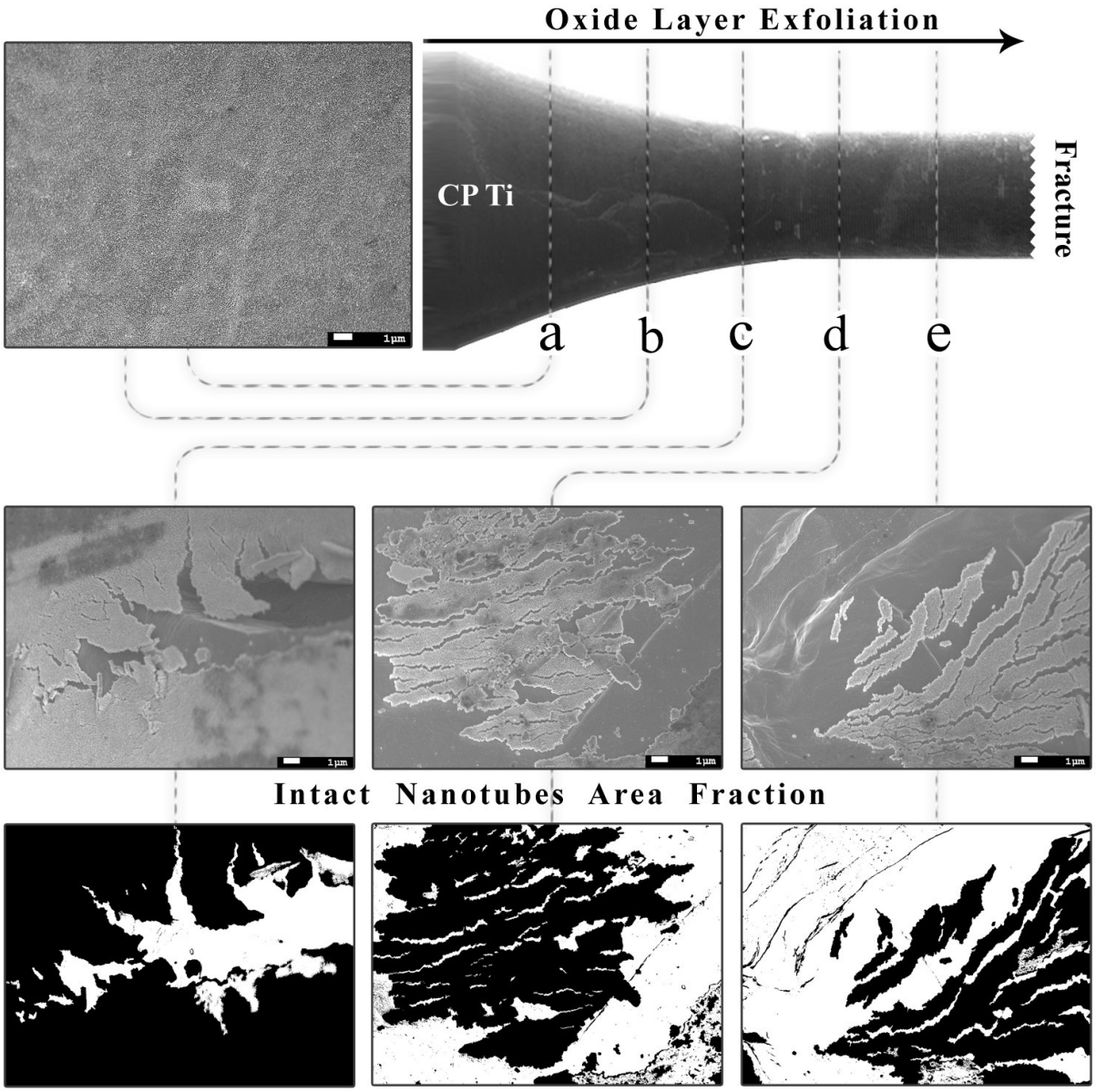

Figure 51. Morphologic analysis of the surface layer (CP Ti) as a function of the position along the sample. Intact nanotubes (a-b), onset and propagation of exfoliation (c-d) and final fracture surface (e). In the lower row the corresponding masks of calculated area fractions obtained by ImageJ software are shown.

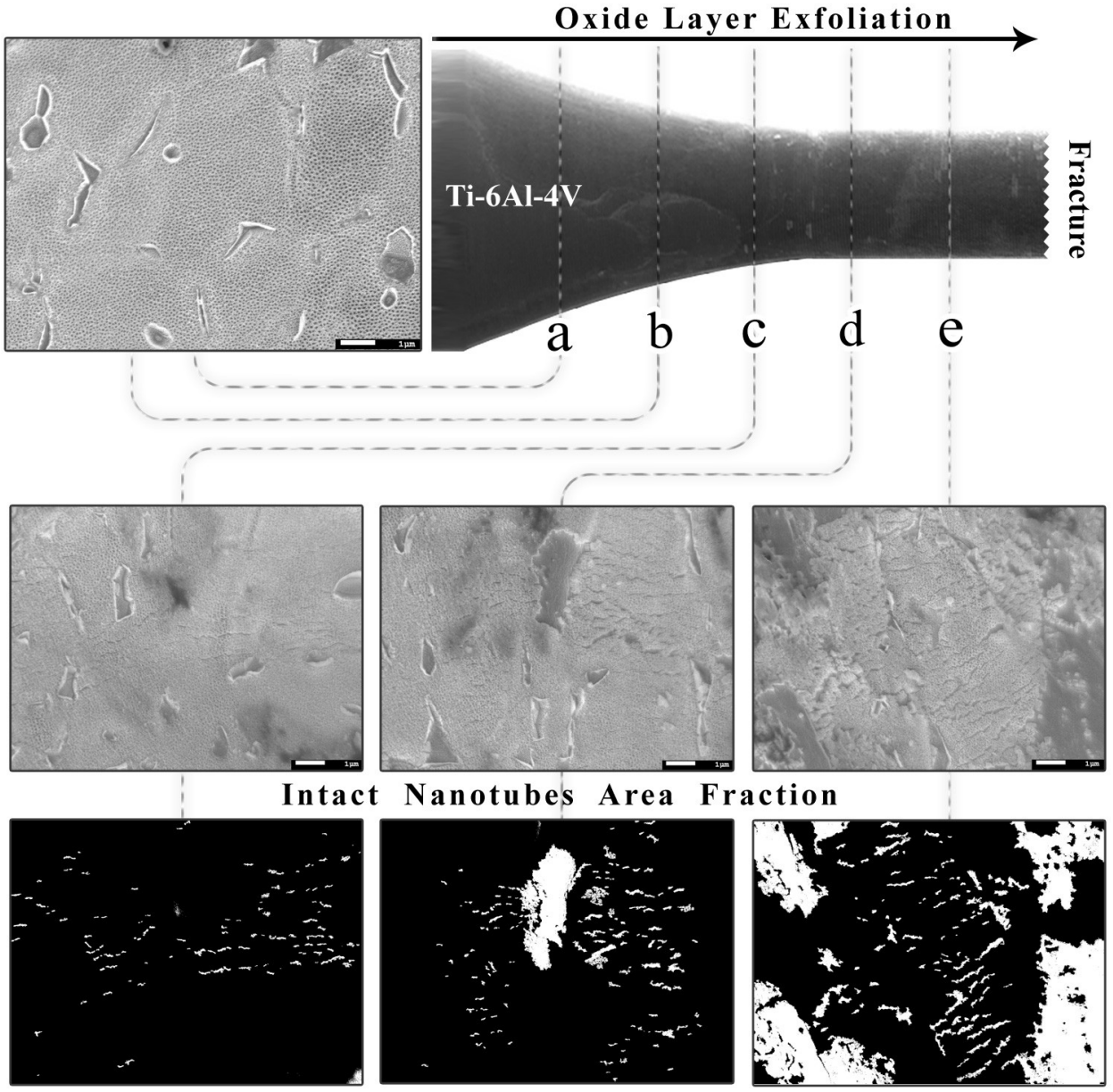

Figure 52. Morphologic analysis of the surface layer (Ti-6Al-4V) as a function of the position along the sample. Intact nanotubes (a-b), onset and propagation of exfoliation (c-d) and final fracture surface (e). In the lower row the corresponding masks of calculated area fractions obtained by ImageJ software are shown.

The area fraction of delaminated nanotubes from the surface of the metal was quantified by ImageJ software and subtracted from the total surface area (figure 53). Only results obtained after statistical analysis (i.e. unpaired t-test) exhibiting a P-value less than 0.05 were considered statistically significant. These results revealed that the higher fractions of nanotubes were flaked off the surface of the CP Ti than that of Ti-6Al-4V. In addition, significant decrease in area fraction of intact nanotubes was found on the surface of CP Ti as moving towards fracture. However, the decrease in area fraction of intact nanotubes on the surface of Ti-6Al-4V was not statistically significant.

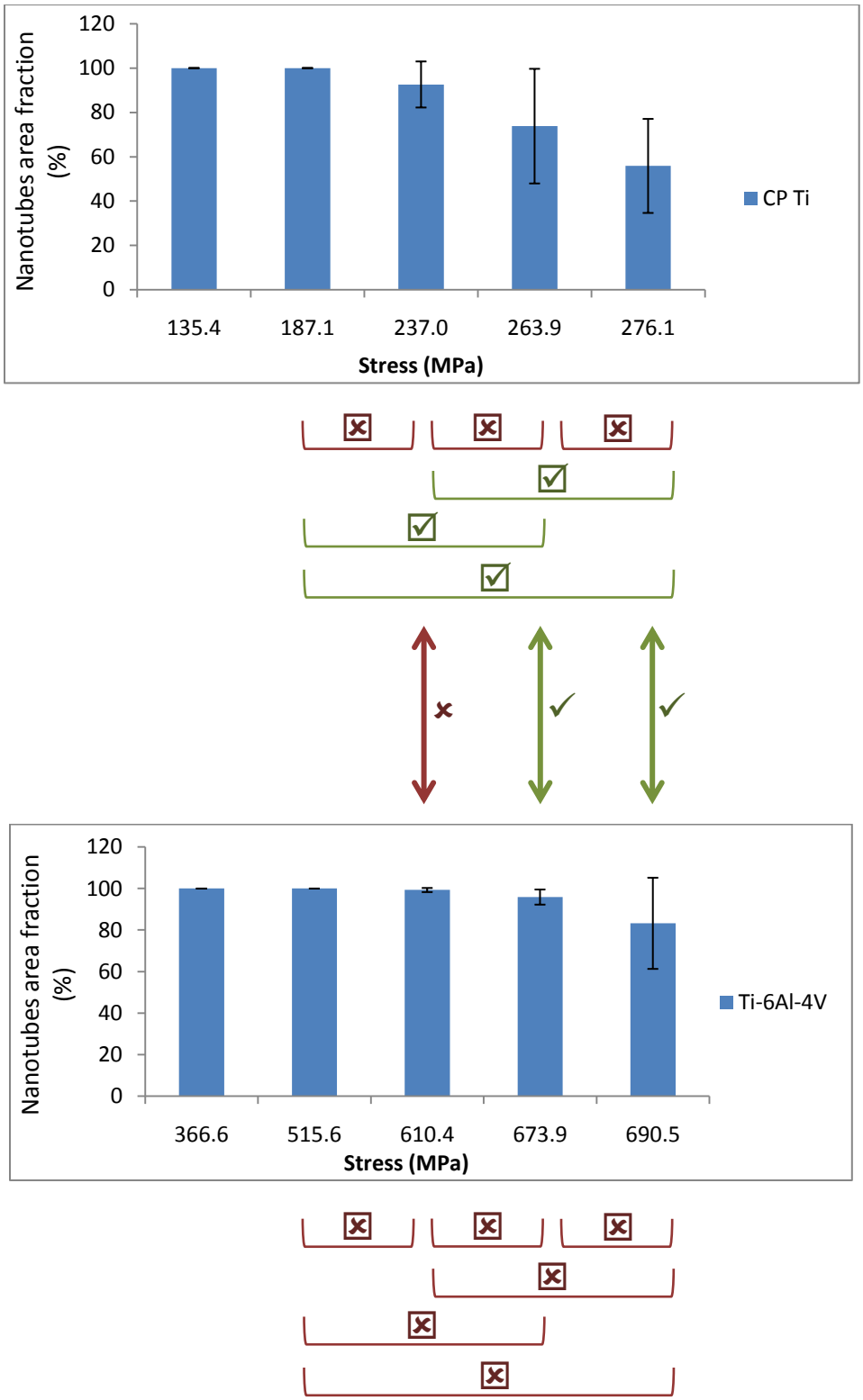

☒ P>0.05 (insignificant difference) ✓ P<0.05 (significantly different)

Figure 53. Area fraction of intact nanotubes, calculated as the ratio between the surface of intact nanotubes and the total surface.

4.1.4.5 Other relevant results: nanopatterning with calcium-based solution

Many studies agree that the development of new techniques to create and control surface nanofeatures of biomedical implants will pave the way for a new generation of biomaterials with "intelligent surfaces" capable of accelerating tissue repair and regeneration, osseointegration, as well as other cellular activities in bone-implant interface [45]. In general, the presence of calcium on the surface of the implant is expected to accelerate the process of bone formation. For this reason, treatments that can nanopattern metals while introducing calcium onto their surfaces are very promising. In this context, calcium-based solutions (table 9) were investigated in relation to their applicability to oxidative nanopatterning and anodization of CP Ti. Surfaces were characterized by SEM, and the presence of calcium assessed by Energy Dispersive X-ray (EDX) measurements.

EDX analysis (Figures 54-55) revealed no evidence of calcium content in any of the mentioned treatments. However, nanometric surface features were visible. Taken together, these results suggest that the solutions adopted are promising to nanopattern titanium, but not suitable for adding calcium. For this, other techniques such as chemical or physical deposition and sputtering may be more efficient.

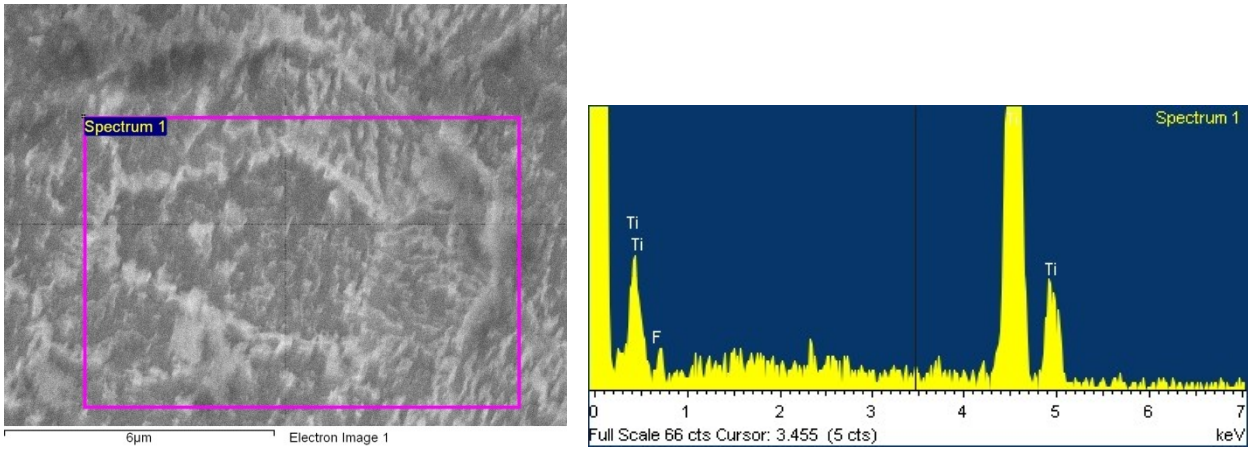

Figure 54. Calcium adsorption evaluation by means of EDX on nanopatterned CP Ti sample.

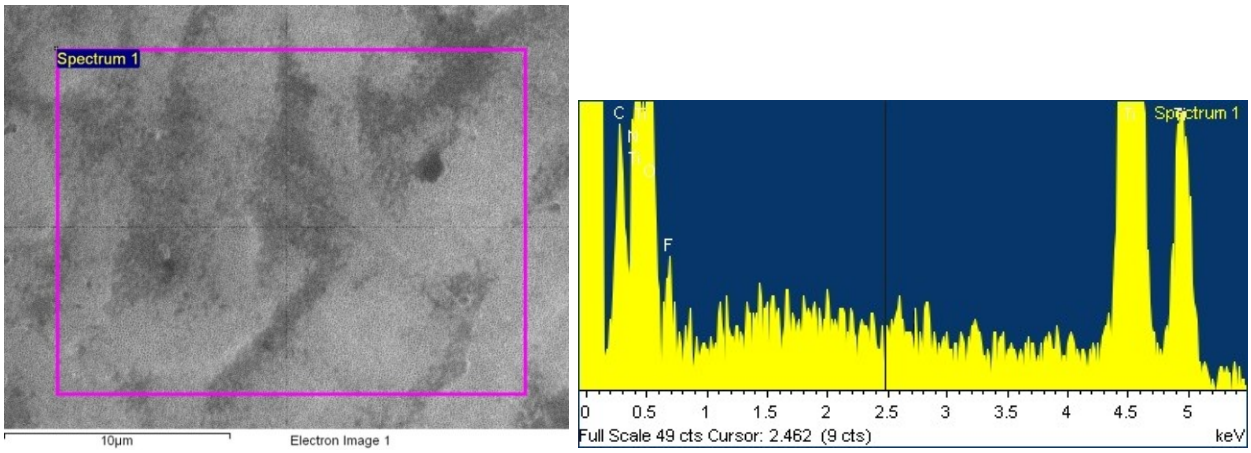

Figure 55. Calcium adsorption evaluation by means of EDX on anodized CP Ti sample.

Chapter 5 Discussion

Our results showed the fabrication of reproducible nano-topographies, nanotubes in case of anodization and nanopores in case of oxidative nanopatterning, on the surface of CP Ti and Ti-6Al-4V. In the case of anodization, as mentioned earlier, characterization of the oxide layer is not considered as one of the goals of this Thesis, yet the diameter and length of the nanotubes and the thickness of the oxide layer were measured. This outcome agrees with previous results found by J. Zhao *et al.* [39] and I. Demetrescua *et al.* [40] that were described in section 2.6.2. Comparing created nanotubes on CP Ti with those on Ti-6Al-4V surfaces, one may notice that anodizing Ti-6Al-4V to 30 minutes and 20 Volts caused preferential etching of the β-phase grains.

In the case of oxidative nanopattterning, the native oxide layer is removed from the titanium surface and this layer is recreated under controlled conditions to stimulate the cellular activities at the nanoscale and to enhance the osseointegration [43]. Achieving the goal of the project, the effect of the oxidative nanopatterning on the fatigue life of the CP Ti and Ti-6Al-4 is evaluated. The main objective of this thesis was to assess the effects of surface treatments on the fatigue resistance of the CP Ti and Ti-6Al-4V. The morphological analysis by means of SEM is presented in section 4.1.4.2. The response of the fatigue resistance of CP Ti to surface modifications oxidative nanopatterning and anodization are represented in S-N curves and

compared to the fatigue resistance of the polished samples (figure 42). These results suggest that anodization and oxidative nanopatterning did not significantly affect the fatigue resistance of CP Ti. In case of anodization, these findings are consistent with previous work of Leinenbach and Eifler that was illustrated in section 2.7.1. The large scattering in fatigue results of polished samples is ascribed to the surface inhomogeneities that exist on the surface of the metal [8]. Leinenbach and Eifler believe that even after polishing, surface microcracks perpendicular to the loading direction still remain on the surface of the material that act as stress concentration points and crack initiation sites and in contrary, anodization results in more homogeneous surfaces and consequently less scattered fatigue curves [8]. Same reasoning holds for oxidative nanopatterning as well. In other words, oxidative nanopatterning created a homogeneous oxide layer on the surface of the metal which resulted in less scattered fatigue behavior.

However, fatigue results of Ti-6Al-4V, in contrary to those of CP Ti, were significantly different. This finding suggests that anodization and oxidative nanopatterning of Ti-6Al-4V decreases the fatigue life of the material. In the event of anodization this result is consistent with the previous studies carried out by W. L. Pigatin Coasta *et al.* and I. Apachitei *et al* [10][9]. In their research I. Apachitei *et al* suggest that the decrease in fatigue limit of anodized Ti-6Al-4V is ascribed to mostly the brittle TiO_2 oxide layer, and also the propagation of pre-existing oxide microcracks and the accumulation of internal stresses during the oxidation process [9]. They believe that the brittle oxide film cracks when subjected to the cyclic loading; these cracks act as stress risers and lead to crack initiation [9]. However, our assessment of fatigue response of surface modified CP Ti proves insignificant effects of oxide layer brittleness on the fatigue life of both materials. Our findings (figure 42) show that the existence of the oxide film on the surface of the CP Ti did not affect the fatigue performance of the material significantly. Moreover, the oxide layer analysis

(section 4.1.4.4) proves that the CP Ti oxide layer is even more brittle than that of Ti-6Al-4V. Therefore, the brittleness of the TiO_2 cannot be the primary reason for fatigue resistance decrease of Ti-6Al-4V. Likewise anodization, oxidative nanopatterning of Ti-6Al-4V in piranha solution had deleterious effects on its fatigue performance.

We believe that the decreased fatigue life of Ti-6Al-4V by both treatments is attributed to higher rate of etching of β-phase grains. Initially in the untreated samples the β-phase grains were as interstitial grains surrounded by the α-phase grains. In the course of anodization and oxidative nanopatterning, the β-grains etched at higher rate and were preferentially removed resulting in the creation of cavities and microscale voids on the surface of the metal. These microscale cavities are considered as stress concentration sites where cracks could initiate and propagate upon fatigue cyclic loading leading to the final fatigue failure of the alloy.

Area fraction decrease of intact nanotubes on the surface of CP Ti and Ti-6Al-4V (figure 53) revealed higher rate of exfoliation of CP Ti oxide layer than that of Ti-6Al-4V. Additionally, one may notice, by observing figures 51 and figure 52 (that illustrate the flow of oxide layer area-fraction-decrease from the furthest point to the closest to the fracture) that area fractions of Ti-6Al-4V nanotubes were measured at higher magnification than that of CP Ti. This further confirms the superiority of adhesion and strength level of Ti-6Al-4V oxide layer than that of CP Ti.

This is ascribed to the higher thickness of the oxide layer in case of CP Ti (i.e. 380±16 nm) than in the case of Ti-6Al-4V (210±13 nm). In addition, based on the provided information in literature, one may claim that Ti-6Al-4V anodized oxide layer has higher adhesion bonding and strength than that of CP Ti. Many researchers have studied the microstructure and morphology of titanium oxide film. Their findings confirm the presence of aluminum and vanadium in the Ti-

6Al-4V oxide layer [62], which increases its strength in comparison to the case of CP Ti. M. Adachi *et al.* have shown that oxide adherence strength of Ti-6Al-4V is higher than that of CP Ti [63]. Furthermore, it is well known that one of the causes of the fatigue failure is accumulation of dislocations and formation of persistent slip bands (PSB) [64]. Dislocation movement is restricted and slip band formation is delayed in Ti-6Al-4V due to presence of fine equiaxed α+β grains. Hence, Ti-6Al-4V experiences less pronounced formation of slip bands and intrusion, extrusions on its surface than CP Ti, which can be counted as another reason for less oxide layer exfoliation in Ti-6Al-4V than in CP Ti.

Chapter 6 Conclusion and outlook

The aim of this thesis was to evaluate the effects of surface treatments on the fatigue resistance of biocompatible metals. It is now widely recognized that biological substrates on which cells thrive consist of nanometric structures and molecular networks, and the sensing apparatus of cells operates on the nanometer scale. Therefore, the selected surface treatments were those that can superimpose nanoscale topographies on the surface of the metal and their effects on improving the biocompatibility of the metal have been proven. Two techniques were chosen, namely anodization and oxidative nanopatterning. By anodization, reproducible uniform arrays of nanotubes structured the oxide layer (TiO_2) on the surface of the two widely used medically relevant metals in biomedical applications that are commercially pure titanium (CP Ti) and Ti-6Al-4V. The thickness of the oxide layer and diameter of the nanotubes were consistent with those of previous work (see section 4.1.2). With oxidative nanopatterning a homogenous network of sponge-like porous nanopits distributed on the surface of the CP Ti and Ti-6Al-4V was created. To assess the effects of the surface treatments on fatigue life, the surface treated samples of CP Ti and Ti-6Al-4V were fatigue tested. Fatigue testing results yielded six S-N (stress-life) curves corresponding to three surface treatments, including polishing, for two metals. These findings revealed that anodization and oxidative nanopatterning do not have significant effects on the fatigue resistance of CP Ti. However, for Ti-6Al-4V, fatigue testing results suggest that anodization and oxidative nanopatterning surface treatments decrease the fatigue life of the

metal. It can be inferred from SEM image analysis that the primary cause of this fatigue resistance decrease is the preferential etching of the β-phase grains. Due to higher rate of etching than α-phase grains, β-phase grains were etched preferentially leading to the creation of microcavities on the surface of the alloy. These micorcavities can act as stress concentration sites where cracks nucleate and propagate resulting in fatigue failure. In a nutshell, nanotexturing the surface of CP Ti by anodization and oxidative nanopatterning to improve its biocompatibility does not affect the fatigue resistance of the metal; however these surface treatments, although stimulating the cellular activities and improving bone regeneration, decrease the fatigue life of Ti-6Al-4V. In addition, these findings also suggest that the deleterious effects of surface treatments on the fatigue life of Ti-6Al-4V were more pronounced in case of anodization, which is attributed to deeper β-phase grains cavities due to harsher etching during the course of anodization than that of oxidative nanopatterning. Moreover, the area fraction of exfoliated nanotubes from the surface of CP Ti and Ti-6Al-4V were measured to analyze the oxide layer behavior fabricated by anodization. Higher adherence and strength of Ti-6Al-4V oxide layer than CP Ti oxide film is inferred, since the area fraction of intact Ti-6Al-4V oxide film was higher than that of CP Ti. To evaluate the possible calcium absorption by CP Ti through anodization and oxidative nanopatterning surface treatments, various calcium-based solutions were utilized. EDX analysis revealed no evidence of calcium particles on the surface of the metals after the treatments. These findings suggest using other techniques to combine nanofeaturing and calcium particles depositions.

Although the presented results have demonstrated the effects of nanoscale surface treatments on the fatigue resistance of biocompatible metals, but all the fatigue tests are performed in air and room temperature, whereas in reality implants are exposed to *in-vivo* condition (i.e. physiological

corrosive environment). Therefore, it is required for future work to assess the effects of surface treatment in simulated physiological media.

Moreover, the optimized thickness of the oxide layer created by anodization is desired. The best thickness length would be the one that although is good enough to improve the biocompatibility and osseointegration, but also does not impose any negative effects on the mechanical properties, such as fatigue resistance, of the implant.

Finally, Range of the loads of the fatigue tests were chosen based on the fatigue testing equipment restriction and sample configuration. However, it is desired to select this range based on the loadings that an implant is exposed to in different physical activities.

References

[1] N. Tran and T. J. Webster, "Nanotechnology for bone materials," *Wiley Interdisciplinary Reviews: Nanomedicine and Nanobiotechnology*, vol. 1, no. 3, pp. 336–351, 2009.

[2] F. Variola, J. Brunski, G. Orsini, P. T. de Oliveira, R. Wazen, and A. Nanci, "Nanoscale surface modifications of medically-relevant metals: state-of-the art and perspectives," *Nanoscale*, vol. 3, no. 2, pp. 335–353, Feb. 2011.

[3] F. Variola, F. Vetrone, L. Richert, P. Jedrzejowski, J.-H. Yi, S. Zalzal, S. Clair, A. Sarkissian, D. F. Perepichka, J. D. Wuest, F. Rosei, and A. Nanci, "Improving Biocompatibility of Implantable Metals by Nanoscale Modification of Surfaces: An Overview of Strategies, Fabrication Methods, and Challenges," *Small*, vol. 5, no. 9, pp. 996–1006, 2009.

[4] F. Vetrone, F. Variola, P. Tambasco de Oliveira, S. F. Zalzal, J.-H. Yi, J. Sam, K. F. Bombonato-Prado, A. Sarkissian, D. F. Perepichka, J. D. Wuest, F. Rosei, and A. Nanci, "Nanoscale oxidative patterning of metallic surfaces to modulate cell activity and fate," *Nano Lett.*, vol. 9, no. 2, pp. 659–665, Feb. 2009.

[5] B. Ercan, E. Taylor, E. Alpaslan, and T. J. Webster, "Diameter of titanium nanotubes influences anti-bacterial efficacy," *Nanotechnology*, vol. 22, no. 29, p. 295102, Jul. 2011.

[6] S. . Teoh, "Fatigue of biomaterials: a review," *International Journal of Fatigue*, vol. 22, no. 10, pp. 825–837, Nov. 2000.

[7] R. V. Noort, "Titanium: The implant material of today," *J Mater Sci*, vol. 22, no. 11, pp. 3801–3811, Nov. 1987.

[8] C. Leinenbach and D. Eifler, "Influence of oxidation treatment on fatigue and fatigue-induced damage of commercially pure titanium," *Acta Biomaterialia*, vol. 5, no. 7, pp. 2810–2819, Sep. 2009.

[9] I. Apachitei, B. Lonyuk, L. E. Fratila-Apachitei, J. Zhou, and J. Duszczyk, "Fatigue response of porous coated titanium biomedical alloys," *Scripta Materialia*, vol. 61, no. 2, pp. 113–116, Jul. 2009.

[10] M. Y. P. Costa, H. J. C. Voorwald, W. L. Pigatin, V. A. Guimarães, and M. O. H. Cioffi, "Evaluation of shot peening on the fatigue strength of anodized Ti-6Al-4V alloy," *Materials Research*, vol. 9, no. 1, pp. 107–109, Mar. 2006.

[11] H. J. Rack and J. I. Qazi, "Titanium alloys for biomedical applications," *Materials Science and Engineering: C*, vol. 26, no. 8, pp. 1269–1277, Sep. 2006.

[12] "ASM Aerospace Specification Metals Inc. | Metal Distributor Supplier Dealer | Titanium | Stainess Steel | Steel | Aluminum | Nickel | Alloys." [Online]. Available: http://www.aerospacemetals.com/. [Accessed: 27-Feb-2013].

[13] *Biodegradable Metals: From Concept to Applications*. .

[14] M. Papakyriacou, H. Mayer, C. Pypen, H. Plenk Jr, and S. Stanzl-Tschegg, "Effects of surface treatments on high cycle corrosion fatigue of metallic implant materials," *International Journal of Fatigue*, vol. 22, no. 10, pp. 873–886, Nov. 2000.

[15] S. D. Cook, F. S. Georgette, H. B. Skinner, and R. J. Haddad, "Fatigue properties of carbon- and porous-coated Ti-6Al-4V alloy," *Journal of Biomedical Materials Research*, vol. 18, no. 5, pp. 497–512, 1984.

[16] G. Lütjering and J. C. Williams, *Titanium*. Springer, 2007.

[17] M. J. Donachie, *Titanium: A Technical Guide*. ASM International, 2000.

[18] H. E. Boyer, *Atlas of Fatigue Curves*. ASM International, 1986.

[19] S. W. Lu, M. Z. Hu, and Y. Gogotsi, *Ceramic Nanomaterials and Nanotechnology III: Proceedings of the 106th Annual Meeting of The American Ceramic Society, Indianapolis, Indiana, USA 2004, Ceramic Transactions*. John Wiley & Sons, 2012.

[20] W. D. Callister, *(WCS)Materials Science and Engineering: An Introduction, 7th Edition Binder Ready Version*. John Wiley & Sons, 2008.

[21] "Mechanics of Materials," *MIT OpenCourseWare*. [Online]. Available: http://ocw.mit.edu/courses/materials-science-and-engineering/3-11-mechanics-of-materials-fall-1999/. [Accessed: 27-Feb-2013].

[22] "Fatigue limit," *Wikipedia, the free encyclopedia*. 26-Feb-2013.

[23] "Fatigue Failures." [Online]. Available: http://www.materialsengineer.com/CA-fatigue.htm. [Accessed: 27-Feb-2013].

[24] U. Krupp, *Fatigue Crack Propagation in Metals and Alloys*. John Wiley & Sons, 2007.

[25] "Lecture Notes | Fracture and Fatigue | Materials Science and Engineering | MIT OpenCourseWare." [Online]. Available: http://ocw.mit.edu/courses/materials-science-and-engineering/3-35-fracture-and-fatigue-fall-2003/lecture-notes/. [Accessed: 27-Feb-2013].

[26] E. S. Puchi-Cabrera, M. H. Staia, C. Tovar, and E. A. Ochoa-Pérez, "High cycle fatigue behavior of 316L stainless steel," *International Journal of Fatigue*, vol. 30, no. 12, pp. 2140–2146, Dec. 2008.

[27] T. Akahori, M. Niinomi, K.-I. Fukunaga, and I. Inagaki, "Effects of microstructure on the short fatigue crack initiation and propagation characteristics of biomedical α/β titanium alloys," *Metall and Mat Trans A*, vol. 31, no. 8, pp. 1949–1958, Aug. 2000.

[28] A. S. Guilherme, G. E. P. Henriques, R. A. Zavanelli, and M. F. Mesquita, "Surface roughness and fatigue performance of commercially pure titanium and Ti-6Al-4V alloy after different polishing protocols," *The Journal of Prosthetic Dentistry*, vol. 93, no. 4, pp. 378–385, Apr. 2005.

[29] F. Javier Gil, J. A. Planell, A. Padrós, and C. Aparicio, "The effect of shot blasting and heat treatment on the fatigue behavior of titanium for dental implant applications," *Dental Materials*, vol. 23, no. 4, pp. 486–491, Apr. 2007.

[30] B. Kasemo, "Biological surface science," *Surface Science*, vol. 500, no. 1–3, pp. 656–677, Mar. 2002.

[31] K. Anselme, "Osteoblast adhesion on biomaterials," *Biomaterials*, vol. 21, no. 7, pp. 667–681, Apr. 2000.

[32] T. S. Price, P. H. Shipway, and D. G. McCartney, "Effect of cold spray deposition of a titanium coating on fatigue behavior of a titanium alloy," *J Therm Spray Tech*, vol. 15, no. 4, pp. 507–512, Dec. 2006.

[33] R. K. Alla, K. Ginjupalli, N. Upadhya, M. Shammas, R. K. Ravi, and R. Sekhar, "Surface Roughness of Implants: A Review," *Trends in Biomaterials and Artificial Organs*, vol. 25, no. 3, pp. 112–118, May 2011.

[34] K. Anselme and M. Bigerelle, "Statistical demonstration of the relative effect of surface chemistry and roughness on human osteoblast short-term adhesion," *J Mater Sci: Mater Med*, vol. 17, no. 5, pp. 471–479, May 2006.

[35] G. M. Whitesides, "Nanoscience, Nanotechnology, and Chemistry," *Small*, vol. 1, no. 2, pp. 172–179, 2005.

[36] F. Variola, F. Vetrone, L. Richert, P. Jedrzejowski, J.-H. Yi, S. Zalzal, S. Clair, A. Sarkissian, D. F. Perepichka, J. D. Wuest, F. Rosei, and A. Nanci, "Improving biocompatibility of implantable metals by nanoscale modification of surfaces: an overview

of strategies, fabrication methods, and challenges," *Small*, vol. 5, no. 9, pp. 996–1006, May 2009.

[37] C. Leinenbach and D. Eifler, "Fatigue and cyclic deformation behaviour of surface-modified titanium alloys in simulated physiological media," *Biomaterials*, vol. 27, no. 8, pp. 1200–1208, Mar. 2006.

[38] S. Minagar, C. C. Berndt, J. Wang, E. Ivanova, and C. Wen, "A review of the application of anodization for the fabrication of nanotubes on metal implant surfaces," *Acta Biomaterialia*, vol. 8, no. 8, pp. 2875–2888, Aug. 2012.

[39] J. Zhao, X. Wang, R. Chen, and L. Li, "Fabrication of titanium oxide nanotube arrays by anodic oxidation," *Solid State Communications*, vol. 134, no. 10, pp. 705–710, Jun. 2005.

[40] I. Demetrescu, D. Ionita, C. Pirvu, and D. Portan, "Present and Future Trends in TiO2 Nanotubes Elaboration, Characterization and Potential Applications," *Molecular Crystals and Liquid Crystals*, vol. 521, no. 1, pp. 195–203, 2010.

[41] S.-H. Oh, R. R. Finõnes, C. Daraio, L.-H. Chen, and S. Jin, "Growth of nano-scale hydroxyapatite using chemically treated titanium oxide nanotubes," *Biomaterials*, vol. 26, no. 24, pp. 4938–4943, Aug. 2005.

[42] K. C. Popat, L. Leoni, C. A. Grimes, and T. A. Desai, "Influence of engineered titania nanotubular surfaces on bone cells," *Biomaterials*, vol. 28, no. 21, pp. 3188–3197, Jul. 2007.

[43] J.-H. Yi, C. Bernard, F. Variola, S. F. Zalzal, J. D. Wuest, F. Rosei, and A. Nanci, "Characterization of a bioactive nanotextured surface created by controlled chemical oxidation of titanium," *Surface Science*, vol. 600, no. 19, pp. 4613–4621, Oct. 2006.

[44] F. Variola, J.-H. Yi, L. Richert, J. D. Wuest, F. Rosei, and A. Nanci, "Tailoring the surface properties of Ti6Al4V by controlled chemical oxidation," *Biomaterials*, vol. 29, no. 10, pp. 1285–1298, Apr. 2008.

[45] P. T. de Oliveira, S. F. Zalzal, M. M. Beloti, A. L. Rosa, and A. Nanci, "Enhancement of in vitro osteogenesis on titanium by chemically produced nanotopography," *Journal of Biomedical Materials Research Part A*, vol. 80A, no. 3, pp. 554–564, 2007.

[46] L. Richert, F. Vetrone, J.-H. Yi, S. F. Zalzal, J. D. Wuest, F. Rosei, and A. Nanci, "Surface Nanopatterning to Control Cell Growth," *Advanced Materials*, vol. 20, no. 8, pp. 1488–1492, 2008.

[47] L. Le Guéhennec, A. Soueidan, P. Layrolle, and Y. Amouriq, "Surface treatments of titanium dental implants for rapid osseointegration," *Dental Materials*, vol. 23, no. 7, pp. 844–854, Jul. 2007.

[48] "Hydroxylapatite," *Wikipedia, the free encyclopedia*. 27-Jan-2013.

[49] C.-C. Chen, T.-H. Huang, C.-T. Kao, and S.-J. Ding, "Characterization of functionally graded hydroxyapatite/titanium composite coatings plasma-sprayed on Ti alloys," *Journal of Biomedical Materials Research Part B: Applied Biomaterials*, vol. 78B, no. 1, pp. 146–152, 2006.

[50] T. Laonapakul, Y. Otsuka, A. R. Nimkerdphol, and Y. Mutoh, "Acoustic emission and fatigue damage induced in plasma-sprayed hydroxyapatite coating layers," *Journal of the Mechanical Behavior of Biomedical Materials*, vol. 8, pp. 123–133, Apr. 2012.

[51] M. Y. P. Costa, M. L. R. Venditti, H. J. C. Voorwald, M. O. H. Cioffi, and T. G. Cruz, "Effect of WC–10%Co–4%Cr coating on the Ti–6Al–4V alloy fatigue strength," *Materials Science and Engineering: A*, vol. 507, no. 1–2, pp. 29–36, May 2009.

[52] L. Pazos, P. Corengia, and H. Svoboda, "Effect of surface treatments on the fatigue life of titanium for biomedical applications," *Journal of the Mechanical Behavior of Biomedical Materials*, vol. 3, no. 6, pp. 416–424, Aug. 2010.

[53] C. Fleck and D. Eifler, "Corrosion, fatigue and corrosion fatigue behaviour of metal implant materials, especially titanium alloys," *International Journal of Fatigue*, vol. 32, no. 6, pp. 929–935, Jun. 2010.

[54] R. A. Zavanelli, G. E. Pessanha Henriques, I. Ferreira, and J. M. D. de Almeida Rollo, "Corrosion-fatigue life of commercially pure titanium and Ti-6Al-4V alloys in different storage environments," *The Journal of Prosthetic Dentistry*, vol. 84, no. 3, pp. 274–279, Sep. 2000.

[55] L. C. Lucas and J. E. Lemons, "Biodegradation of Restorative Metallic Systems," *ADR*, vol. 6, no. 1, pp. 32–37, Sep. 1992.

[56] P. K. Vallittu and M. Kokkonen, "Deflection fatigue of cobalt-chromium, titanium, and gold alloy cast denture clasp," *The Journal of Prosthetic Dentistry*, vol. 74, no. 4, pp. 412–419, Oct. 1995.

[57] M. Nakagawa, S. Matsuya, T. Shiraishi, and M. Ohta, "Effect of Fluoride Concentration and pH on Corrosion Behavior of Titanium for Dental Use," *J DENT RES*, vol. 78, no. 9, pp. 1568–1572, Sep. 1999.

[58] "Molecular Expressions Microscopy Primer: Anatomy of the Microscope - Microscope Optical Components." [Online]. Available: http://micro.magnet.fsu.edu/primer/anatomy/componenthome.html. [Accessed: 27-Feb-2013].

[59] "ZEISS Microscopy Online Campus | Microscopy Basics | Image Formation." [Online]. Available: http://zeiss-campus.magnet.fsu.edu/articles/basics/imageformation.html. [Accessed: 27-Feb-2013].

[60] S. S. Dheda and F. A. Mohamed, "Effect of initial microstructure on the processing of titanium using equal channel angular pressing," *Materials Science and Engineering: A*, vol. 528, no. 28, pp. 8179–8186, Oct. 2011.

[61] E08 Committee, "Practice for Conducting Force Controlled Constant Amplitude Axial Fatigue Tests of Metallic Materials," ASTM International, 2007.

[62] S. Szmukler-Moncler, T. Testori, and J. P. Bernard, "Etched implants: A comparative surface analysis of four implant systems," *Journal of Biomedical Materials Research Part B: Applied Biomaterials*, vol. 69B, no. 1, pp. 46–57, 2004.

[63] M. Adachi, J. R. Mackert, E. E. Parry, and C. W. Fairhurst, "Oxide Adherence and Porcelain Bonding to Titanium and Ti-6A1-4V Alloy," *J DENT RES*, vol. 69, no. 6, pp. 1230–1235, Jun. 1990.

[64] "Fatigue Crack Initiation." [Online]. Available: http://www.ndt-ed.org/EducationResources/CommunityCollege/Materials/Structure/fatigue.htm. [Accessed: 27-Feb-2013].

[65] H. Lee, S. Mall, and W. Y. Allen, "Fretting fatigue behavior of shot-peened Ti–6Al–4V under seawater environment," *Materials Science and Engineering: A*, vol. 420, no. 1–2, pp. 72–78, Mar. 2006.

Appendices

A1. Effect of surface modifications on the fatigue life of Ti-based metals.

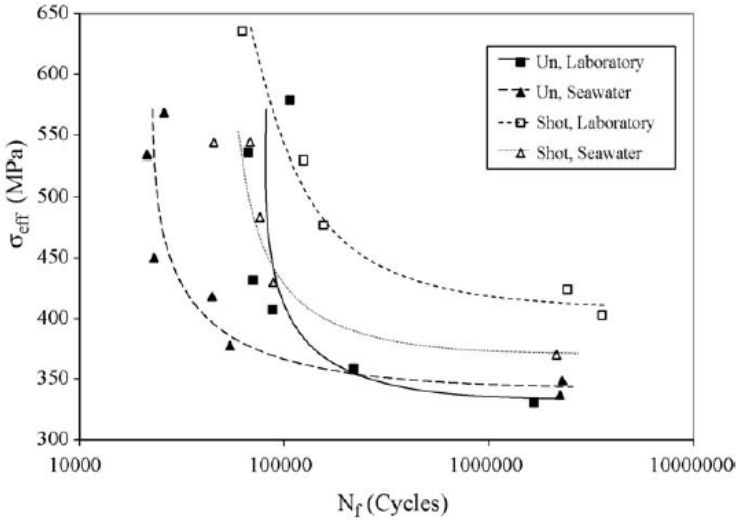

Figure 56. Effect of shot peening on fatigue performance of Ti-6Al-4V [65].

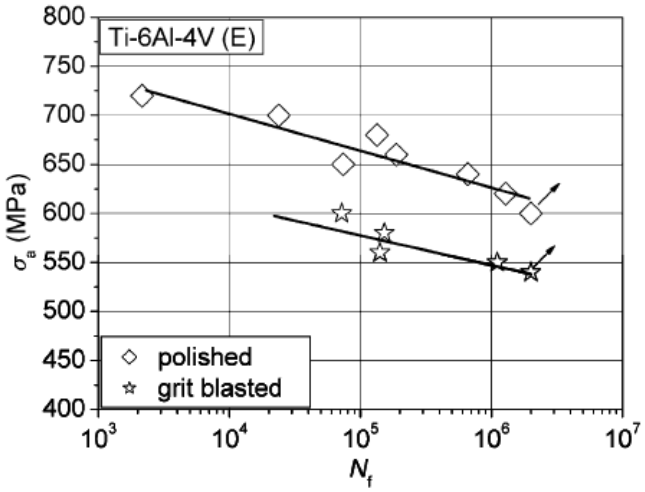

Figure 57.S-N curves of polished and grit blasted Ti-6Al-4V in Ringer's solution [37].

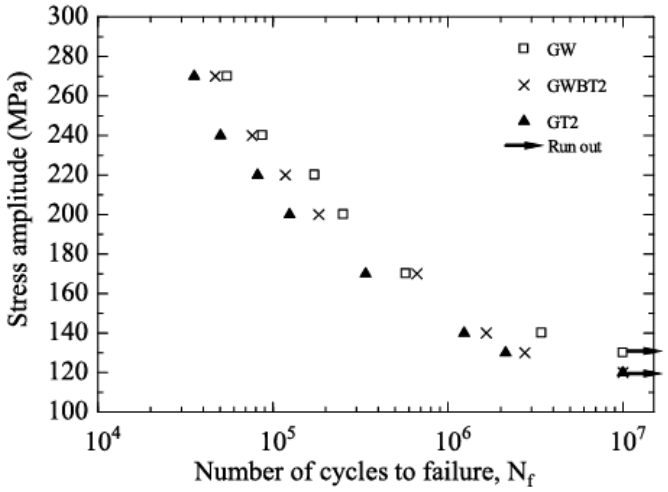

Figure 58.Fatigue behavior of grit blasted (GW), grit blasted and HA coated (GT2), grit blasted and HA/Ti coated [50].

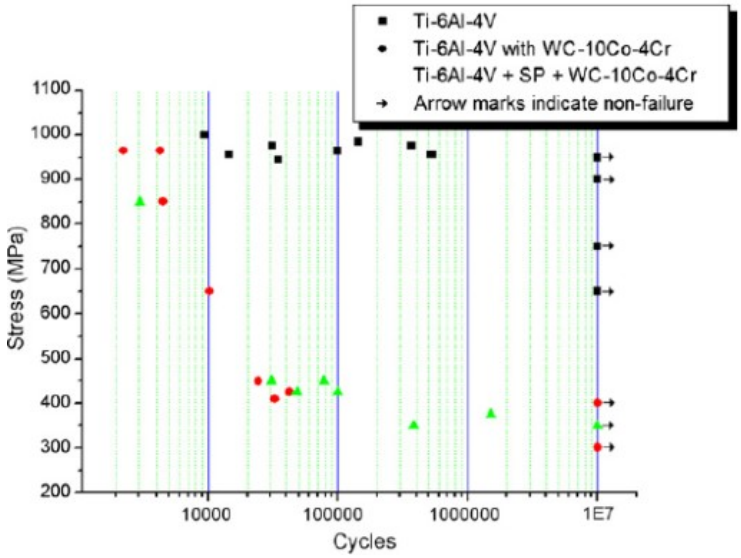

Figure 59. Fatigue performance of Ti-6Al-4V with WC–10%Co–4%Cr coating, and prior shot peening (SP) [51].

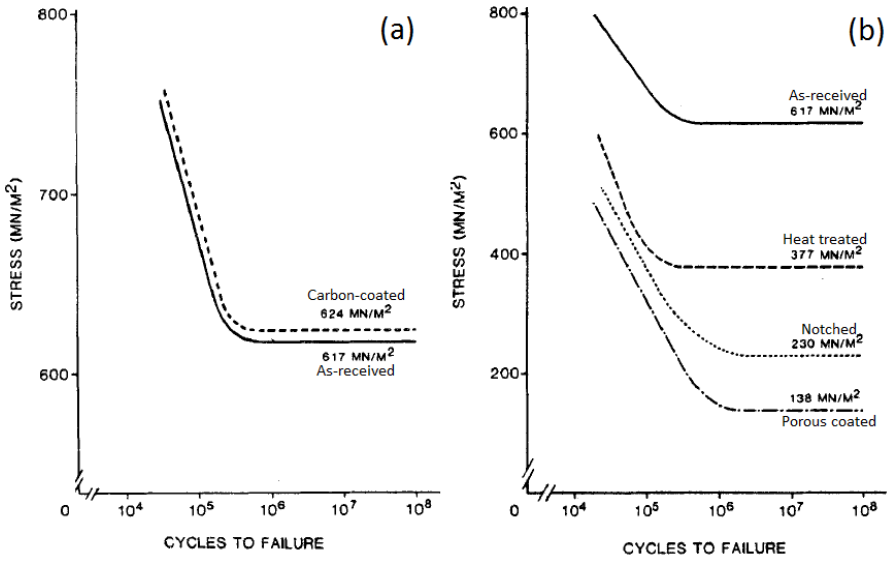

Figure 60. Fatigue performance of Ti-6Al-4V with different treatments [15].